CFD modelling of axial fans for thermal management applications

RANDI FRANZKE

CFD modelling of axial fans for thermal management applications
RANDI FRANZKE

"A fool is a man who never tried an experiment in his life."
– Erasmus Darwin

CFD modelling of axial fans for thermal management applications

Randi Franzke
Department of Mechanics and Maritime Sciences
Chalmers University of Technology

Abstract

Reducing CO_2 emissions is one of the key challenges in todays automotive industry. Different strategies to achieve this goal are, for example, to electrify the power-train and to reduce the aerodynamic drag by reducing the amount of cooling air through the underhood. In order not to sacrifice the cooling performance, a better understanding of the air flow through the underhood compartment is necessary. Computational Fluid Dynamics (CFD) is an important tool for the investigation of the underhood flow, since it gives the possibility to look at the flow field even in areas where measurement equipment cannot reach. This work focusses on the simulation of the main driving factor of underhood flow: the axial cooling fan.

In CFD multiple methods of varying complexity are available to simulate the fan rotation. The more computational expensive approach, called the Rigid Body Motion (RBM), physically resolves the rotation, while the less expensive approach, called the Multiple Reference Frame (MRF), rotates the air in proximity to a stationary rotor around the blades. In the first study presented in this thesis, the flow field downstream of an axial fan is investigated for these two methods and in addition, a third hybrid approach is also evaluated. The results are compared to experimental data, which were obtained in the Volvo Cars Model-scale Wind Tunnel by using Laser Doppler Anemometry. In the second study, the interaction between the MRF approach and different upstream and downstream conditions were investigated. For this study, a temperature variation upstream of the rotor is introduced, as well as different geometric obstacles up- and downstream.

As a result of the presented investigations it could be confirmed that the RBM approach gives the best representation of the flow field downstream of the fan. The MRF on the other hand showed severe limitations that the users need to be aware of. Especially the rotation of an upstream temperature source, that was found in Paper II, can lead to misleading results of component temperatures. However, when the temperature field is uniformly distributed or of minor importance, the MRF is still the most feasible approach for large applications.

Acknowledgements

The work presented in this thesis would not have been possible if it had not been for a number of people who guided and supported me throughout the past years. First of all, I would like to thank my supervisor (and finally also examiner) Prof. Simone Sebben for her valuable input and constructive criticism to my writing. Second, I would like to thank the people involved in the project, namely Emil Willeson and Alexander Broniewicz from Volvo Car Corporation for their support. A special thank you goes to Tore Bark from Volvo Cars, who always had an open ear and open mind for numerous technical (and close to philosophical) discussions about basic fluid dynamics and CFD.

Next, I would like to thank my manager Mats Löfman and my colleagues at the Cooling Performance & Heat Management group at Volvo Cars, who always were welcoming me back with open arms, no matter how long I have been neglecting them for being at Chalmers.

Furthermore, I want to thank my former and present colleagues and friends at Chalmers for creating such a pleasant and friendly work environment. A special thanks goes to the RVAD group for many interesting discussions on- and off-topic; my friends from the Vehicle Dynamics group and my office-neighbour and friend Sina for always listening and all the after-works. Also, I want to thank Sonja for always being helpful, supportive and bringing us all together!

Last but not least, I want to thank my family and Rico for always supporting and encouraging me. Without your support and encouragement I probably would not have ended up where I am now.

<div align="right">

Randi Franzke
Gothenburg, June 2019

</div>

List of included papers

This thesis consists of the following papers. References to the papers will be made using Roman numerals.

I. Franzke, R., Sebben, S., *Validation of Different Fan Modelling Techniques in Computational Fluid Dynamics.* Proceedings of the 21st Australasian Fluid Mechanics Conference, Adelaide, 2018.

II. Franzke, R., Sebben, S., Bark, T. and Willeson, E., *Evaluation of the Multiple Reference Frame Approach for the Modelling of an Axial Cooling Fan.* Submitted to: International Journal of Automotive Technology, 2019.

The author of this thesis was responsible for conducting the experiments and simulations, as well as analysing the results and writing the papers. The co-authors contributed with supervision, technical discussions and review of the manuscripts.

Table of Contents

INCLUDED PAPERS

Nomenclature

Symbol	Unit	Description
d,D	m	Diameter
f	1/s	Frequency
k	m^2/s^2	Turbulent kinetic energy
l,L	m	Length
$\dot{m}$	kg/s	Mass flow rate
$\vec{r}$	m	Radial position
$\vec{v}$	m/s	Velocity vector
x,y,z	m	Position in global reference frame
ε	m^2/s^3	Turbulent dissipation rate
λ	nm	Wave length
$\vec{\omega}$	rpm	Rotational vector

Abbreviations

BEV	Battery Electric Vehicle
BSA	Burst Spectrum Analyser
CFD	Computational Fluid Dynamics
DES	Detached Eddy Simulation
HEV	Hybrid Electric Vehicle
ICE	Internal Combustion Engine
IDDES	Improved Delayed Detached Eddy Simulation
LDA	Laser Doppler Anemometry
LES	Large Eddy Simulation
MRF	Multiple Reference Frame
MWT	Model Wind Tunnel
PVT	*Personvagnars Vindtunnel* (referring to the full-scale wind tunnel at Volvo Cars)
PWM	Pulse Width Modulation
RANS	Reynolds-averaged Navier Stokes
RBM	Rigid Body Motion
SGS	Sub-grid Scale
VCC	Volvo Car Corporation

Chapter 1

Introduction

1.1 Background

The introduction of vehicles with various degrees of electrification is aimed at reducing the negative impact individual transportation has on the climate. Many governments have, therefore, started to ban diesel engines and to give incentives to individuals to buy electrified cars. This has lead in the past year to a significant reduction in new registered diesel cars (-17.9 %), and an increase in chargeable electrified vehicles (+40 %) in the European Union [1]. A large factor that seems to hinder people to switch from an internal combustion engine (ICE) vehicle to an electrified one is the so-called "range anxiety", i. e. the fear of running out of battery on a longer trip, requiring to take a longer break while the battery is charging. A way to extend the range of the vehicle is to improve its energy efficiency, e. g. by improving the aerodynamic design and thus lower the aerodynamic drag. One measure to reduce the aerodynamic drag is to minimize the cooling airflow through the underhood. This can, for example, be achieved by reducing the grille size or by using active grille shutters that can be closed when no ram air is needed for sufficient cooling. Electric cars have already a lower need for external cooling air, since the temperatures in the underhood compartment are considerably lower compared to a vehicle with a conventional internal combustion engine. However, the components of the electric driveline are very sensitive to high temperatures and their efficiency is largely related to their operating temperature. Additionally, the packaging in both conventional and electrified cars has become tighter over the years. An extreme case are

hybrid electric vehicles (HEV) that need to accommodate the components for a conventional (ICE, high temperature) driveline and an electric (low temperature) one. The proximity of high temperature equipment and heat sensitive components makes smart packaging even more important. Moreover, the cooling of the components still needs to be sufficient in cases with low ram air flow, such as in hill climbing with trailer and when the car is idling ("stop-and-go" traffic). In these situations, the flow is driven through the underhood compartment with the help of a cooling fan.

In current vehicle development, both experimental and computational tools are used. For thermal management, measurements are commonly limited to the measurement of temperature in the air, on component surfaces and of the cooling liquids. Flow measurements have been proven to be difficult to achieve, due to the complex and narrow environment of the engine bay, which limits the accessibility [4]. However, it is still of interest to know the amount of cooling air entering the underhood compartment. A common way to obtain this value is by measuring the air flow through the radiator instead. This can be done by using vane anemometers [3], pressure probes [26] or performing force measurements on the complete radiator [14]. An overview of different techniques can be found in [20]. However, these measurements do not give any information about flow behaviour in the engine bay. Therefore, simplified set-ups, that provide a controlled environment and good accessibility, are often studied. A design of a simplified engine bay is proposed by Khaled et al. [17], with optical access for performing Laser Doppler Anemometer and Particle Image Velocimetry measurements [16], while especially for studies of the engine cooling fan a plenum-rig set-up is preferred [7, 9, 19]. The benefit of a plenum rig is, that either the mass flow through or the pressure difference over the radiator and/or cooling fan can be directly controlled, which allows for the investigation of test cases along the whole fan performance curve.

Computational Fluid Dynamics (CFD) is an important tool when it comes to underhood thermal management. Not only can it be used in early design phases, when no prototypes are available, but it can also provide a complete overview of the flow and temperature field inside the engine bay. However, the accuracy of these simulations is highly dependent on a number of factors, such as the mesh resolution, the implemented models and solvers. Therefore, it is important to know the limitations and possibilities of the different settings.

1.2   Scope and Objective

This work is part of a larger project, aiming at obtaining a better understanding of underhood flow in order to improve current simulation methods at Volvo Cars. Since the underhood flow is very complex, due to the large amount of components involved, the focus of this thesis is put, initially, on the axial cooling fan. This component is deemed to have a large influence on the underhood flow in general, and its performance is crucial for an effective thermal design.

The main tool of investigation in this thesis is CFD, supported by validation measurements performed with Laser Doppler Anemometry, done on an isolated fan. The two most common ways of simulating rotation in CFD, the Multiple Reference Frame (MRF) method and the Rigid Body Motion (RBM) approach, are studied. The flow fields obtained by these two methods are compared with each other and validated by measurements. A third approach is presented, called average MRF, which aims at improving the flow field results from the standard MRF method, while retaining its low computational costs. In a next step, the interactions of the MRF model with its surroundings were investigated. This was done by looking at the transport of the temperature field through the MRF region and the interaction between the MRF model with different geometries upstream and downstream of the fan.

The results obtained by these studies allow to better understand the abilities and limitations of different fan modelling techniques in CFD.

Chapter 2

Background

The following chapter aims at introducing the industrial context of the thesis and elaborate the background of numerical and experimental methods used. Section 2.1 gives a short introduction to the underhood environment and the challenges of thermal management. Section 2.2 introduces the working principles of the different methods for fan modelling, which are evaluated in this work, and gives a brief overview of previous works. Finally, Section 2.3 describes the measurement principle of Laser Doppler Anemometry (LDA) and its usage in previous studies on the underhood flow.

2.1 Vehicle Thermal Management

Thermal management is an important dimensioning factor for the performance of road vehicles. It needs to be appropriately designed in order to provide the necessary cooling and heating of the driveline components, even in extreme driving conditions, and ensuring that component and fluid temperatures are within set requirements. For vehicles with an internal combustion engine, typical driving conditions that usually serve as test cases for the thermal management systems (such as the cooling fan) are: hill-climb with trailer, high speed driving and thermal soak. The first case puts a high load on the propulsion system while having only a limited amount of cooling air flow due to ram air. The second case has both a high load on the propulsion system and a high availability of external cooling air. The third case, thermal soak, usually occurs when the vehicles comes to a stand still after a high load
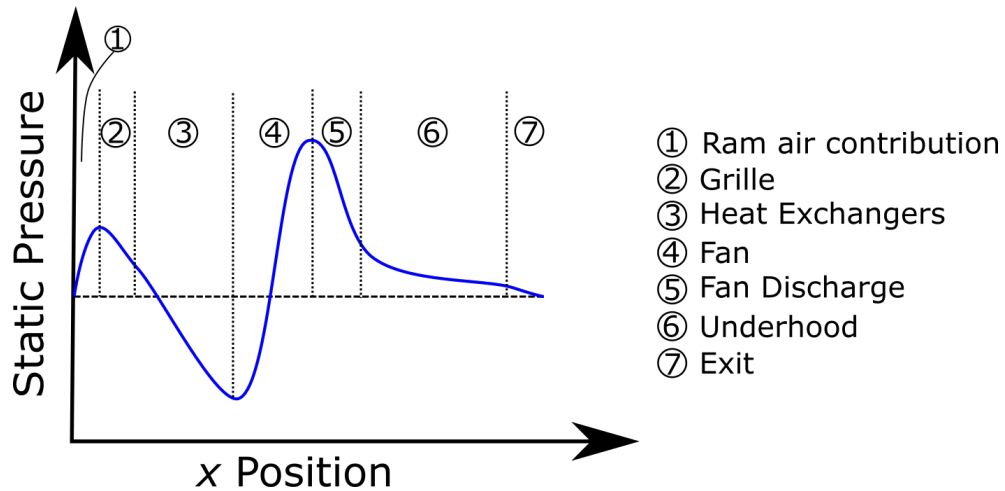
Figure 2.1: *Static pressure curve over the length of the engine bay.*

condition, and only the cooling fan can drive external cooling air through the underhood region. The operation of the fan can also be necessary in other (low-speed) driving cases to compensate for the pressure losses occurring due to the heat exchangers and other components in the engine bay. Figure 2.1 represents the static pressure curve over the course of the underhood length.

The choice of the vehicle cooling fan is usually made by looking at the fan performance curve, which gives the pressure rise over the fan for the range of volume flow rates that the fan can provide. An example of such a curve is given in Figure 2.2. The performance curve is specific for a given fan, rotor diameter and rate of rotation, and is usually provided by the fan supplier. The fan performance curves can be scaled for different rotational rates and diameters with the so-called fan laws, as long as the rotor geometry itself is constant.

For electrified vehicles, thermal management remains an important attribute, since the electric components are very sensitive to the local temperature regarding their efficiency and lifetime. Extreme temperatures, both hot and cold, can affect the operating conditions and lead to inefficient behaviour. Excessively high temperatures reduce the lifetime of the components. In a hybrid electric vehicle (HEV), components of both the electric driveline and the ICE powertrain coexist in the underhood compartment. Therefore an improved understanding of how the hot and cold airstreams are directed in the underhood is crucial.
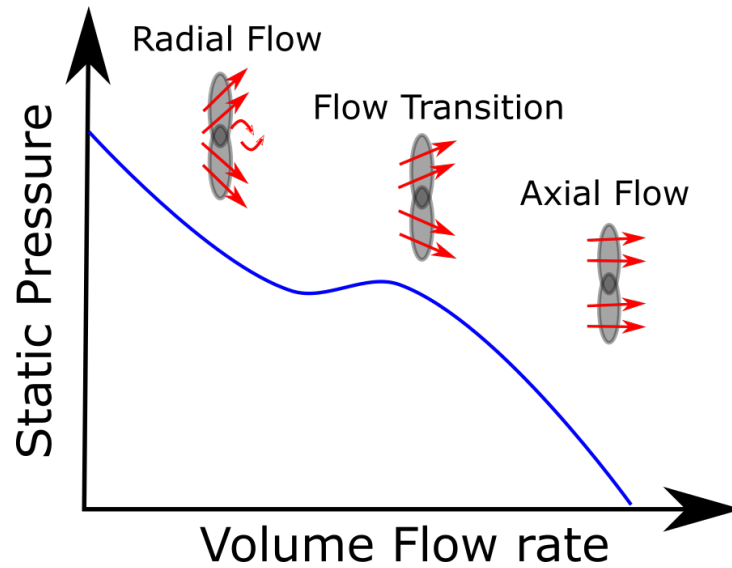
Figure 2.2: *Exemplary fan performance curve.*

2.2 Fan Modelling

There are multiple methods that can be used to model the rotation of a fan in CFD, which vary in the amount of included detail and computational effort. These methods can be separated into two categories: one-dimensional and three-dimensional.

One-dimensional methods can be used to represent the pressure rise over the fan region using the fan performance curve (see Figure 2.2). These methods have the benefit of being fairly simple and relatively inexpensive to use and implement. The downside, however, is that the fan performance curve for the given fan needs to be measured in advance and since it is a 1-D representation, no 3-D effects, such as flow swirls, can be captured [5]. Therefore, these techniques are mainly found in applications where computational resources are limited or short lead time is a crucial factor.

With increasing computational power, 3-D methods that include the rotor geometry and therefore no longer require the fan curve, have become more feasible for a larger range of applications. The two most common methods to model rotation are the *Multiple Reference Frame (MRF)* method, sometimes also known as the *Moving Reference Frame* or the *Frozen Rotor* approach, and the *Rigid Body Motion (RBM)* method, sometime referenced as the

Sliding Mesh (SM) method. Both methods are described in the following sections. Additionally, a hybrid approach is presented, which is referred to as the *Averaged MRF* (avgMRF) method. This hybrid approach was first proposed by Gullberg et al. (2011) and is applied in this study with some modifications [8].

Multiple Reference Frame (MRF)

The *Multiple Reference Frame* model, is the most common approach for inexpensive modelling of translation and/or rotation of parts in CFD. Its major benefit is that it is a steady-state method, and therefore does not require a large amount of computational resources. The geometry (in this case the fan blades) is not physically moved, but instead the air velocity in a specified region is transformed into a moving reference frame. Thereby, the air moves around the stationary rotor blades instead of the rotor blades moving through the non-rotating air, as is illustrated in Figure 2.3. Hence, this method is sometimes also referenced as the *Frozen Rotor* approach. The sense of rotation of the air is therefore also opposed to the sense of rotation of the blades. The velocity vector in the new (rotating) reference frame becomes:

$$\vec{v}_{\mathrm{MRF}} = \vec{v} - \vec{\omega} \times \vec{r}$$

where $\vec{v}$ is the velocity vector in the global (stationary) reference frame, $\vec{\omega}$ is the rotational rate and $\vec{r}$ is the radial position.

All governing equations in the "rotating" region are then solved in the new reference frame. By transforming the velocity into the moving reference frame, additional source terms for the centripetal and Coriolis acceleration are added to the RANS momentum equations [13].

A limitation to this approach is that all surfaces that are included in the MRF domain, but stationary in the global reference frame, need to be rotational symmetric with respect to the axis of rotation [8], thereby limiting the size of the MRF domain. Another challenge is that MRF simulations have specific requirements on the interfaces between the stationary and the moving reference frame. Over these interfaces, also the flow conditions need to be rotationally symmetric, so only axial and radial dependencies of the velocity are allowed [32]. If tangential dependencies were present, the flow conditions for one or multiple blades would differ from the rest. This would mean that the results are dependent on the position of the frozen rotor, which has been
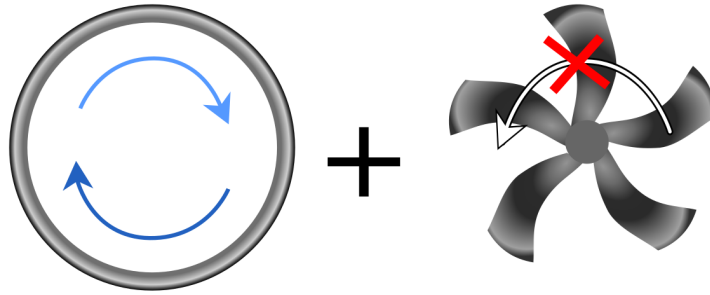
Figure 2.3: *Illustration of the MRF approach: the rotor remains stationary, while the air moves around the blades in a specified region.*

shown in [8] for a case where an asymmetric engine mock-up was placed downstream of a rotor. Previous studies have been dealing mainly with the prediction of the fan performance curve, when using the MRF approach. Gullberg et al. [10] found that for an axial fan without a ring connecting the fan tips (a so-called open fan), the fan performance curve is commonly 14 % under-predicted. The differences are smaller, when the fan operates in axial conditions, i.e. at high volume flow rates. For the radial and transitional regime, the error in predicting the curve is larger.

Different investigations by Wang et al. (2005), Kobayashi et al. (2011), Gullberg et al. (2011) and Peng et al. (2018) looked into the effect of the length and shape of the MRF domain on the prediction of the pressure rise over different volume rates [31, 11, 18, 27]. The authors of these studies found that placing the upstream MRF interface further away from the blades gives more uniform inflow conditions, and therefore less deviation between the measured fan performance curve and the experimentally obtained one. For open fans, a larger radial extent downstream of the fan had also been shown to be beneficial, since it helps capturing the vortex structures originating from the blade tips. For closed fans, there are no tip vortices, and therefore the radial extend is less important [12].

However, the fan domain sizes that the authors of these studies suggest, are usually difficult to accomplish for automotive applications. A vehicle cooling fan is often positioned just a few centimetres downstream of the radiator and is hold by struts that are placed downstream of the fan, thus the space on both sides is very narrow.

In spite of these difficulties in correctly applying the MRF approach, MRF is still a popular method due to its comparatively easy set-up and its ap-

plicability in steady-state simulations. Areas of application for this method, are apart from the engine cooling fan [31] also cooling of electric components [28], ventilation [21, 36], tidal turbines [23] and the rotation of wheels in automotive applications [33, 15].

Rigid Body Motion (RBM)

The *Rigid Body Motion*, also known as the *Sliding Mesh*, approach is a more physical approach to fan rotation. Similar to the MRF method, the user specifies a region around the rotor, which should only contain rotating parts and stationary parts that are rotational symmetric. It is an unsteady approach and the volume mesh of the specified fan region is rotated for each time step. This makes the RBM approach computationally more expensive, but also more accurate than the MRF model.

The process is illustrated in Figure 2.4: the blue region is the stationary air field, with nodes at the interface to the rotating fan region (yellow). The nodes that are interacting with each other have the same colour as the region they belong to. If the fan region is rotated due to an advancement in time, the yellow nodes are sliding against the (stationary) blue ones. The flow field data is then interpolated over the interface between the stationary and the rotating region. However, this interpolation can lead to numerical inaccuracies when part of the flow structures are truncated in the process. Therefore it is commonly recommended not to rotate the fan region by more than $1°$ per time step, which presents a major drawback of this approach. Depending on the set-up, however, larger time steps can be possible [22].

If implemented correctly, the results are very close to experimental data and interactions between rotating and stationary parts can be well resolved. In contrast to the MRF approach, there are no requirements on the steadiness or rotational symmetry of the flow field at the interface. Therefore, the RBM approach performs well at all volume flow rates and the region around the rotor can be chosen small.
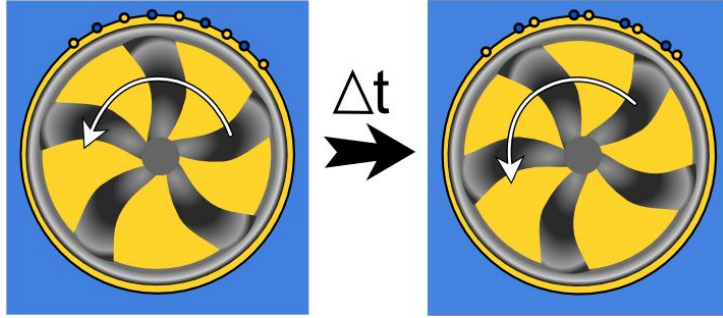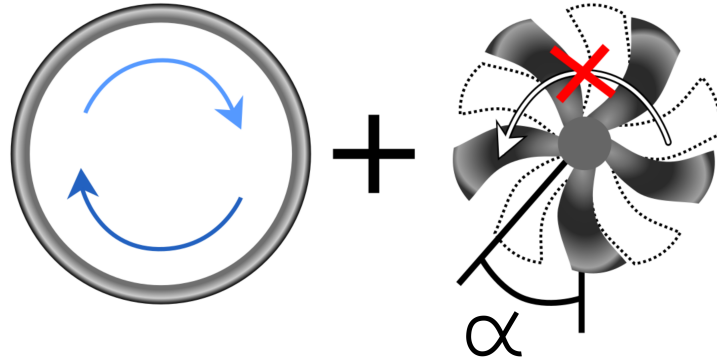
Figure 2.4: *Illustration of the RBM approach, where the outer region (blue) is stationary in the global reference frame, and the fan region (yellow) rotates with every time step. The nodes on the top interface illustrate the movement of the mesh nodes.*

Average MRF

This approach is inspired by Gullberg et al. (2011) who showed that the prediction of the fan performance curve improves for medium to high volume flow rates when averaging it over three different fixed rotor positions [8]. In this thesis, this technique is used to investigate if the effect of the frozen rotor on the flow field, present when using the standard MRF method, can be eliminated.

The principle is illustrated in Figure 2.5: a steady-state simulation is run with the standard MRF approach, and the resulting flow field is saved. Then the whole fan region volume mesh is rotated by a small angle α, another steady-state MRF simulation is run, and the flow field is again saved. This procedure is repeated until the geometry repeats itself, which is for a symmetric rotor geometry after one blade passage, or for a non-symmetric fan after one full rotation ($360°$). Since the position of the blades only has changed slightly by an angle α, merely a small amount of additional iteration steps is needed before the simulation is converged after each rotation. The result is a mean flow field, which does not show any unrealistic uneven behaviour from the blades wake, like it is the case for the standard MRF method.

Figure 2.5: *Illustration of the Average MRF approach, where multiple MRF simulations are performed successively and the flow fields are averaged over all positions.*

2.3 Laser Doppler Anemometry

Laser Doppler Anemometry (LDA), sometimes also referred to as Laser Doppler Velocimetry, is a non-intrusive flow measurement technique. The working principle is illustrated in Figure 2.6. A coherent laser beam is separated by wave length and split into two, in order to ensure coherence between the two beams. Those two beams are then crossing in the measurement point, creating an interference pattern. A seeding particle passing through the measurement point will reflect the interference pattern in a frequency that is proportional to its velocity perpendicular to the axis of the two beams:

$$f_s = v_x \frac{2 \sin \phi}{\lambda_0},$$

where f_s is the superposition of the two scattered beams, v_x is the velocity component perpendicular to the crossed beams, ϕ is the angle between the two beam and λ_0 is the incoming wave length. The orientation of the particles movement can be determined by putting a frequency shift on one of the laser beams, using a so-called Bragg-cell. Due to the frequency shift, the interference pattern in the measurement point will move into one direction, so that particles of equal velocity but different direction create a signal with a difference in frequency. The reflected light is caught by a receiver, which in this configuration is also sitting in the emitting probe ("backscatter"-mode). The signal is then enhanced by a photomultiplier and converted into an
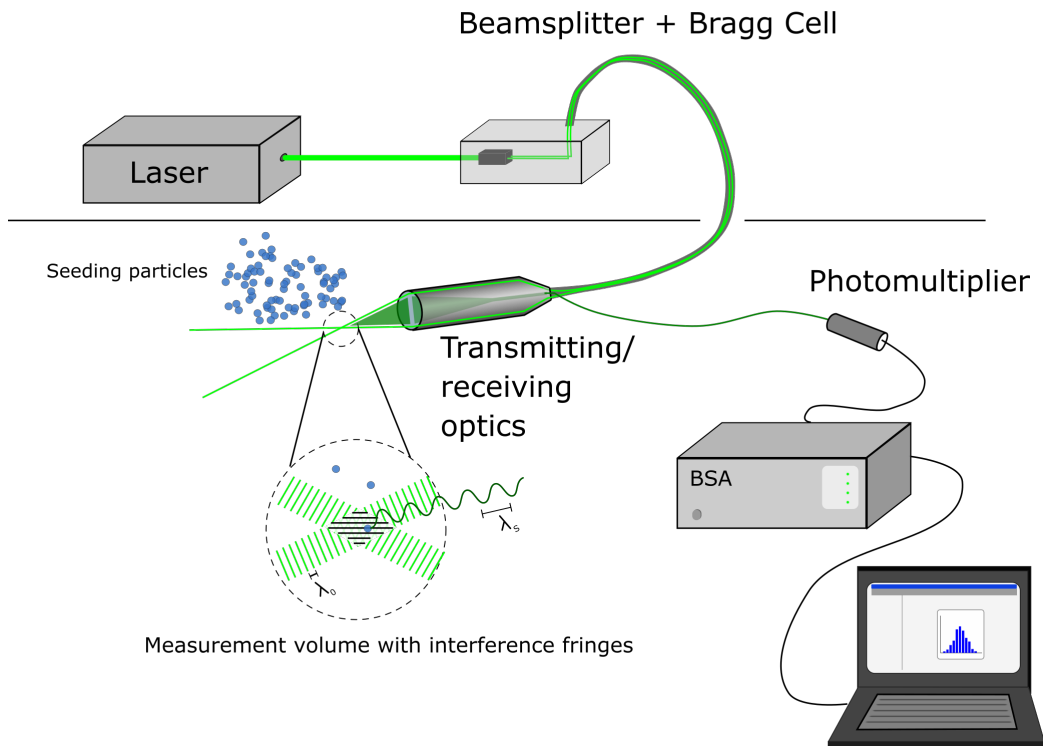
Figure 2.6: *Measurement principle of Laser Doppler Anemometry.*

electric signal, which can via a processor ("Burst Spectrum Analyser", BSA) be send to a computer for data acquisition and analysis.

For the investigation of the flow field around an axial cooling fan and inside an engine bay, LDA presents multiple advantages compared to other measurement techniques. First, the measurement probe is not placed directly in the measurement point. Depending on the focal length of the probe, the device can be placed as far or close from the measurement point as it is desired. For engine bay flow, this is important, since the available space is already limited and it might often not be possible to insert a probe where measurement data is needed. Second, LDA does not have angular dependencies as compared to pressure probes or hot-wire anemometers, which reduces the error and is beneficial, when the direction the inflow is unknown. Third, LDA can acquire time-resolved measurement data, given a high seeding density/sample

rate. And finally, the equipment does not require calibration [2].

Different studies, where LDA has been used to study underhood and/or fan flow, have been performed amongst others by Cogotti and Berneburg (1991) [4] and (1993) [3], Khaled et al. (2012) [17] and (2016) [16] and in aeroacoustic fan development from Zenger et al. [34].

Cogotti and Berneburg have performed one of the few documented experimental studies on the underhood flow of a complete vehicle with the objective to use the measurements for CFD validation. In their first study they used a 2-D LDA probe to investigate the flow downstream of the cooling fan of an Opel Vectra, and around the lambda probe in the rear part of the engine bay, and found that 3-D measurements are imperative to understand the complex flow behaviour. Therefore, for their second study, the authors developed a 3-D probe together with Dantec Dynamics. With the new probe they were able to investigate the complete flow field downstream of an axial fan in an actual underhood environment. Khaled et al. designed a simplified underhood geometry to experimentally investigate the effect of different engine blockage ratios on the flow behaviour downstream of an axial fan with a 2-D LDA probe. Their main conclusions were that the flow induced by an isolated fan in a rig is showing considerably different behaviour from one that is placed in a simplified engine bay. Placing the engine mock-up further away from the cooling unit increased the mass flow through the fan and radiator and therefore increased the cooling performance. The main difficulty in their experimental set-up was that the LDA probe was placed outside of the simplified engine bay. Therefore a larger focal length was needed to reach the measurement place, meaning an increased beam spacing, which in turn limited the the minimal distance between the fan and the engine mock-up.

Methodology

In this chapter the different experimental and numerical set-ups, which were used in the presented studies, are described.

3.1 Experimental Set-up

The experimental part of this study was performed in the model-scale wind tunnel (MWT) of the Volvo Car Corporation (VCC). This wind tunnel is a 1:5 scale version of the full scale wind tunnel (PVT) and was initially used to design the full-scale wind tunnel. The model-scale wind tunnel is of closed-loop type with slotted walls and has a cross section of $0.82 \times 1.32\,\mathrm{m}^2$ (HxW) in the test section. It has a maximum speed of $54\,\mathrm{m/s}$ in the test section and is equipped with a turntable and a distributed boundary layer suction system upstream of the turntable. The removed air is fed back to the system through a distributed blowing system on both sides of the test section behind the slots [25]. For this study, however, the slots were taped over in order to create a closed test section that could more easily be recreated in the CFD simulations later on. Also, the distributed suction system was not activated. The aim of this experimental study was to obtain a set of measurement data that could later be used for the validation of different fan simulation methods. Therefore, an axial cooling fan was mounted centrally in the test section (see Figure 3.1). Since the shroud is non-symmetric, it was chosen to place the fan axis in the centre of the cross section in order to allow the downstream flow to equally expand in y and z-direction (see cut A-A in Figure 3.2).
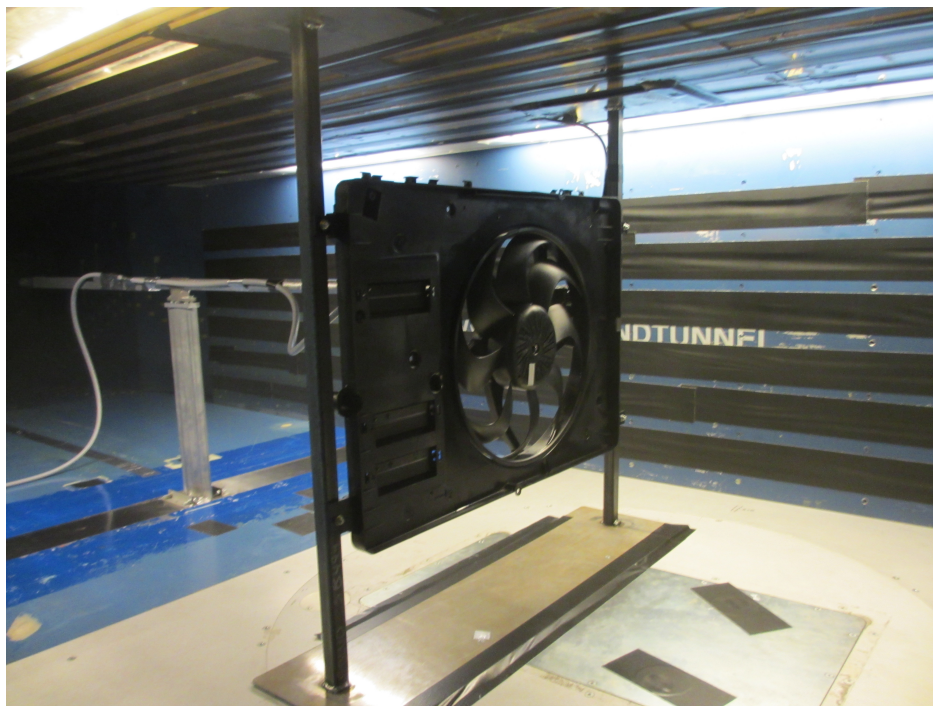
Figure 3.1: *Test section of the MWT with mounted fan shroud and the LDA system on a traverse behind it.*
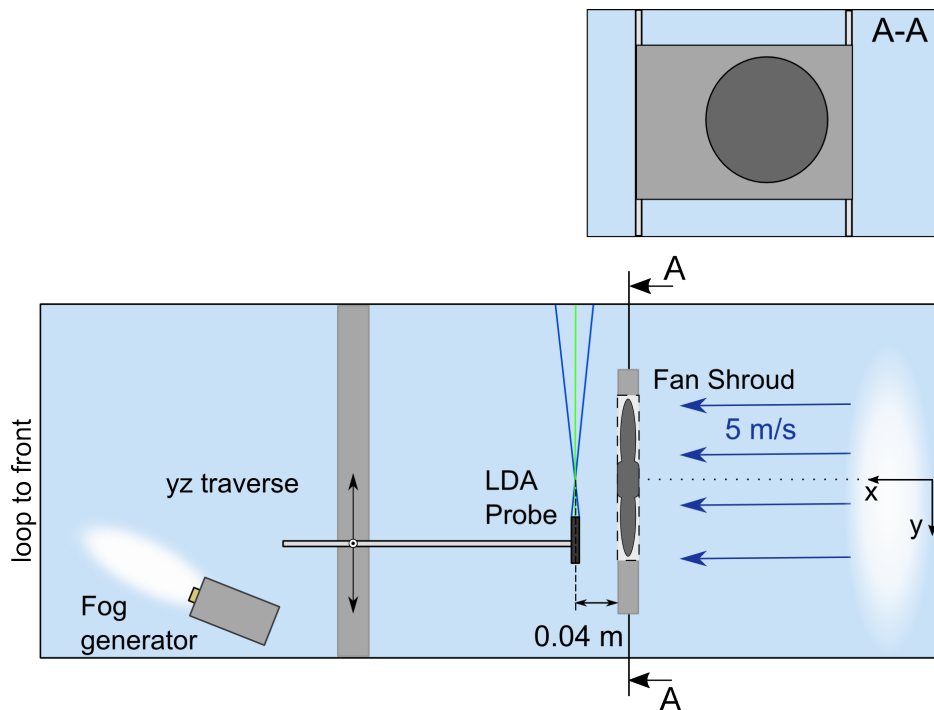
Figure 3.2: *Schematic overview of the experimental set-up in the VCC model wind tunnel.*

The flow measurements were performed with a Laser Doppler Anemometer system by Dantec Dynamics. The probe has a diameter of $d = 14\,\mathrm{mm}$ and a length of $l = 120\,\mathrm{mm}$, and was mounted on a y-z-traverse located $x = 0.04\,\mathrm{m}$ downstream of the fan. It is a two-component probe, being able to measure two velocity components simultaneously, by using two pairs of laser beams with different wave lengths (488 and 514.5 nm). In the presented set-up, this allowed for the measurement of the x and z-component of the velocity vector. The probe has a focal length of 50 mm. The measurement in each point was performed for 10 s or until 10 000 particles passed through the measurement volume. The sample rate that was aimed for was 1000 Hz, which is according to the manufacturer a preferred setting when measuring mean velocities [6]. The seeding particles were generated by a fog machine placed downstream of the traverse. Since the wind tunnel is of a closed-loop type, the fog generator could be placed downstream of the fan, thereby allowing the particles to diffuse over the cross section of the wind tunnel before reaching the fan again. Hence, a more uniform seeding particle distribution could be achieved. The seeding fluid was a water-glycol mixture that is vaporised by the fog generator. The fan used in this set-up was an axial cooling fan in its production shroud (see Figure 3.3). It had eight forward swept blades and a diameter of $D = 0.38\,\mathrm{m}$. The motor was mounted in the hub and hold in place by four struts which are placed downstream of the fan blades. In addition, there was a control unit placed in the flow downstream of the fan. The shroud has three bypass flaps, which were taped closed, to facilitate the comparison to the numerical simulations. The rotation of the fan was realised by connecting it to a DC power supply, and controlling the rotational rate with a pulse-width-modulation (PWM) controller. The PWM controller creates a square wave that switches the power on and off. By defining the frequency and cycle width of the source, the amount of power to the motor can be controlled and the fan speed set. The rotational rate of the fan was checked with an optical tachometer multiple times during the measurement.

In this study, the wind tunnel was run at a constant speed of 5 m/s and the fan was run at two different rotational rates (1400 and 2800 rpm). The wind tunnel speed was chosen to be representative for the flow velocity through the heat exchangers of a car travelling at 70 km/h, which is the typical vehicle test speed for hill-climb with trailer conditions. Depending on the driving conditions (up- or downhill, with or without trailer), the fan speed can vary between zero and full speed. The tested fan rotational rates represent one case close to full speed (2800 rpm) and half of it (1400 rpm).
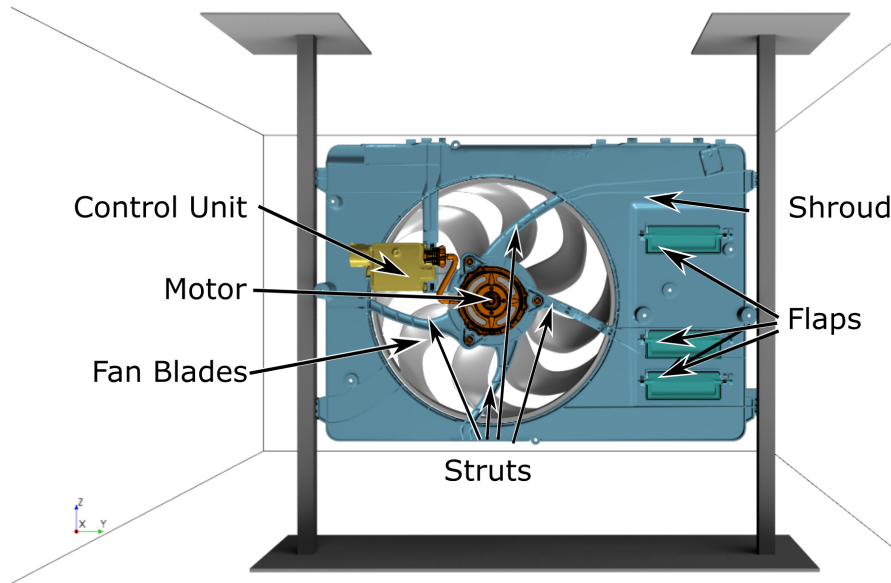
Figure 3.3: *Fan and fan shroud as seen from behind.*

This set-up has some limitations. First, the air is still able to bypass the fan, therefore only the operation at one operating point is possible. Second, the traverse only moves in y and z-direction, limiting the measurement planes to the ones parallel to the shroud. Third, only two velocity components could be measured at the same time. For the third component, the probe would have been to be rotated, which implicates a large uncertainty on measuring in the same point. Finally, the rotational rate could only be indirectly applied and needed to be checked multiple times during the measurement to account for fluctuations in the wind tunnel speed, which would also affect the rotational rate. The accuracy of the measurements was checked by measuring the velocity profile downstream of the fan five times for $5\,\mathrm{m/s}$ at a rotational speed of $1400\,\mathrm{rpm}$. It was found that the average standard deviation along the profile was $\pm 0.3\,\mathrm{m/s}$.
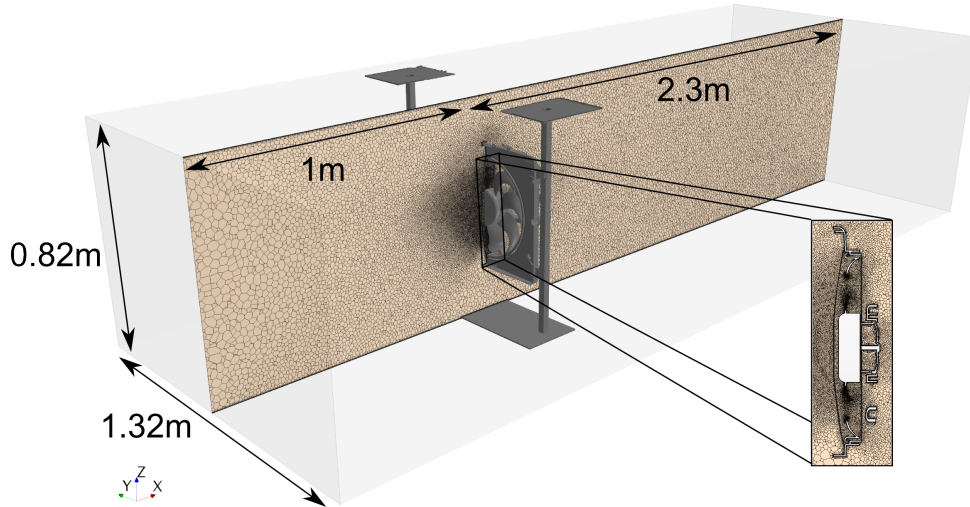
3.2   Numerical Set-up

Two different computational domains were used in this thesis. The first was a cuboid domain, representing the model wind tunnel (MWT) from the experimental study. This set-up was used in Paper I. The second set-up was a pipe with a single fan and a heat source, used in Paper II. All simulations were performed with the commercial Navier-Stokes solver Simcenter StarCCM+.

3.2.1   Model Wind Tunnel Set-up

The first computational domain was an approximate representation of the Volvo Cars model-scale wind tunnel, which has been described in Section 3.1. The numerical model has the same size in cross section, but no representation of the slotted walls, since those have been taped over in the experimental set-up. The numerical domain was reduced to an extended test section, since modelling the complete loop of a wind tunnel only increases the complexity of the set-up but does not improve the results in the test section [24]. The cross section in the numerical model was the same as in the physical MWT. In length, the computational domain extends 1 m upstream and 2.3 m downstream of the mounted fan in order to allow the flow to settle before the outlet. The computational domain can be seen in Figure 3.4.

The computational domain was split into two interfaced regions, one fitted closely around the fan and one in the remaining domain. Both regions are meshed with a polyhedral mesher, resulting into 7.8 million cells in the fan domain and 5 million cells in the air domain. This gives a total of approximately 13 million cells. Special care was taken when meshing the surface of the fan blades, in order not to create any sharp edges. A polyhedral mesh was chosen due to its good applicability for multi-directional flow and that a conformal mesh would be created at the interfaces between the air and the fan region [29].

The inlet boundary condition was set to be a uniform velocity inlet of 5 m/s (same as for the experimental set-up), the outlet boundary was set to be of pressure outlet type. The floor, roof and side-walls were set to adiabatic wall boundaries with no-slip condition.

Figure 3.4: *Numerical set-up for an axial cooling fan mounted in a domain equivalent to the Volvo Cars Model Wind Tunnel (MWT) test section.*

3.2.2 Pipe Set-up

The second set-up, used in Paper II, is a circular pipe with a diameter slightly larger than the fan diameter D. The computational domain can be seen in Figure 3.5. The fan geometry was the same as in the previous set-up. However, in this case the fan was free-floating in the domain, since no shroud or strut geometries were included. The tube extended $2.5\,D$ upstream and $5\,D$ downstream of the fan. Half a diameter upstream of the fan a uniform heat source was introduced, which extended over the lower half cross section of the pipe. The heat source emitted a total power of $5\,\text{kW}$, in order to create a notable temperature difference compared to the ambient temperature.

In this set-up, the computational domain was split into three interfaced regions: the fan domain, the heat source region and the remaining pipe. The fan zone extended over the whole cross section of the pipe, so that all flow had to pass through it. The mesh in the fan domain was a polyhedral mesh with 2.65 million cells. The heat source and the air side were meshed with a trimmed cell mesher, amounting to 2.33 million cells. This gave an amount approximately 5 million cells in total. A mesh study was performed and is presented in Paper II. In this study the trimmed cell mesher was chosen over
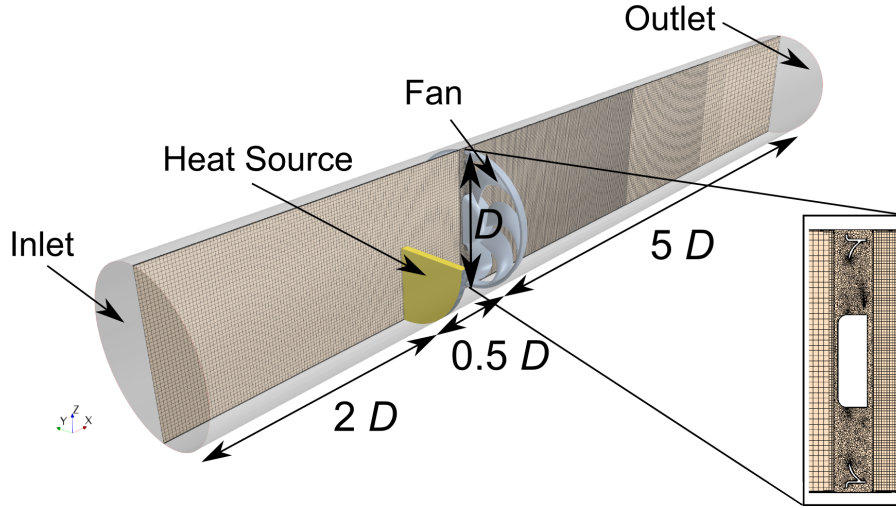
**Figure 3.5:** *Computational domain for the pipe set-up.*

Table 3.1: *Overview of configurations tested in the pipe set-up.*

Case	L_{MRF}[mm]	Rotational Rate [rpm]	Obstruction
Baseline	60	2800	–
T1	60	1400	–
T2	120	2800	–
F1	60	2800	Cylinder (upstream)
F2	60	2800	Cylinder (downstream)
F3	60	2800	Box (downstream)

the polyhedral mesher, since it gives a better control over mesh refinement zones.

Table 3.1 shows an overview of all cases investigated. The baseline case had a length of the MRF domain of $L_{\mathrm{MRF}} = 60\,\mathrm{mm}$ and was run with a fan speed of 2800 rpm. This set-up was chosen, since it is similar to how the fan MRF would be implemented in a vehicle simulation model, with the MRF interfaces sitting close around the rotor and the fan running at high speed. In the second case, T1, the MRF domain was the same as in the baseline case, but the rotational rate was reduced to 1400 rpm to investigate any dependency on the rotational rate. In case T2 the rotational rate was increased again to 2800 rpm and the length of the MRF zone was now doubled

(a)   **(b)**   **(c)**
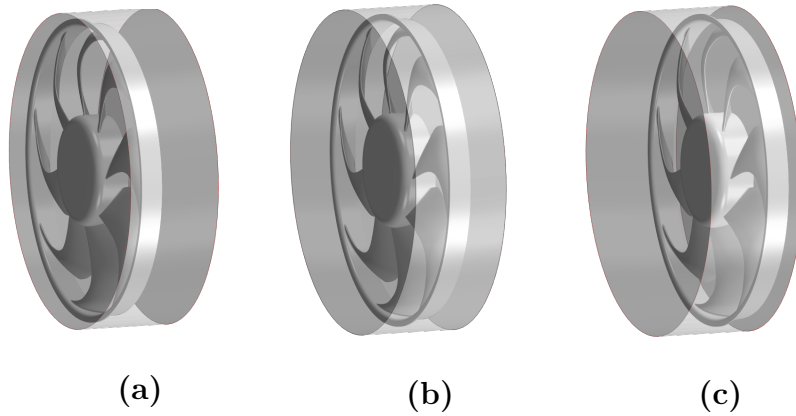
Figure 3.6: *Placement of the MRF zone in relation to the fan blades (case T2): (a) upstream interface close to the blades, (b) equal distance between blades and up-/downstream interface, (c) blades close to the downstream interface.*

($L_{\mathrm{MRF}} = 120\,\mathrm{mm}$). Additionally, it was investigated if there was an effect on the relative position between the up- and downstream interfaces to the blades. The configurations can be seen in Figure 3.6. The rotor was placed in the same position in the global reference frame for all three cases, and the positions of the interfaces were adjusted. In case T2a the rotor had the same distance to the upstream interface as in the baseline configuration, in case T2b it was placed equidistant to both up- and downstream interface and in case T2c the distance between rotor and downstream interface is as in the baseline configuration, with an increased distance to the upstream interface. In the second part of the investigation (cases F1-F3), the MRF domain and the rotational rate were the same as for the baseline case. Here, different obstacles were placed up- and downstream of the MRF interfaces. The implemented geometries are simple, but close to shapes that can be found around a cooling fan in an actual engine bay. In case F1, a cylinder of diameter $d = 20\,\mathrm{mm}$ was positioned one diameter upstream of the upstream MRF interface. The same cylinder was placed one diameter downstream of the MRF downstream interface in case F2. Finally, a cuboid box was placed closely downstream of the MRF zone, representing a control unit similar to the one in Paper I (see Figure 3.3).

(a) *Case F1*   (b) *Case F2*   (c) *Case F3*
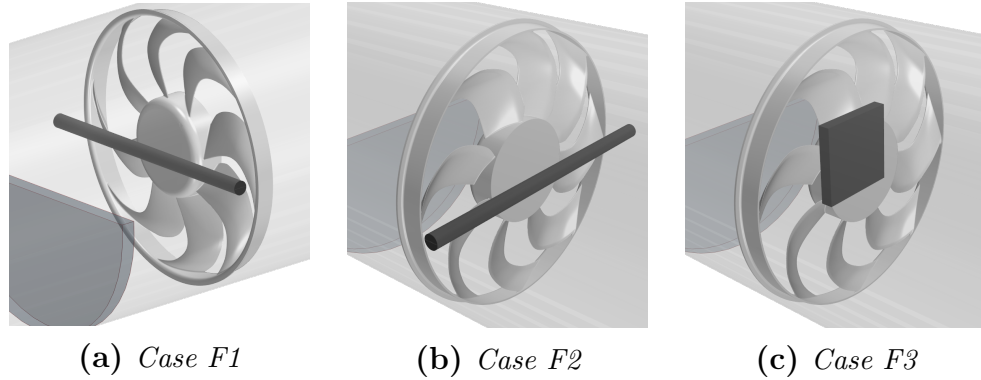
Figure 3.7: *Placement of different obstacles up- and downstream of the MRF interfaces.*

3.2.3 Governing Equations and Turbulence

The CFD code used in this study is Simcenter StarCCM+, a Navier Stokes solver. The governing equations can be found in the literature [30, 29] and are therefore not further discussed here. The steady-state simulations were performed by solving the Reynolds-averaged Navier Stokes (RANS) equations. In the Reynolds-averaging process, the Reynolds stress terms are added as additional unknowns to the momentum equation. In order to close the system of equations, additional equations in the form of turbulence models are necessary.

In this study, the two-layer Realisable k-ε model was used in the steady-state simulations in both set-ups. This model was chosen for its simplicity and due to its good applicability for rotating and swirling flows [35]. In this approach, the turbulent dissipation rate ε is specified in the near wall region as an algebraic function of the turbulent kinetic energy k, and by solving the transport equation for ε far away from the wall. The transport equation of the turbulent kinetic energy is solved throughout the whole flow domain.

In Paper I, the unsteady simulations were performed solving the unsteady RANS (URANS) equations, with the same Realisable k-ε turbulence model. For the unsteady simulations in Paper II, the solver was switched from RANS to Improved Delayed Detached Eddy Simulation (IDDES). This approach is a hybrid approach between Large Eddy Simulation (LES) and URANS. In areas where the mesh fulfils the requirements, LES is performed and large structures are resolved instead of being modelled. In other areas, especially

in the boundary layer, the URANS equations are solved with a chosen sub-grid scale model (SGS). In this case, the Spalart-Allmaras SGS model was chosen due to its known accuracy in boundary layer flows [35].

The mesh around the rotor blades was designed to yield a $y^+ < 1$ under all conditions, i.e. the boundary layer is resolved, and the transport equations are solved down to the respective wall.

In both studies, the time-step for the rotational rate of 2800 rpm was set to $\Delta t = 5.5 \times 10^{-5}$ s and for 1400 rpm it was set to $\Delta t = 1.1 \times 10^{-4}$ s. This time step is equivalent to a rotation of the fan blades of less than $1°$. For one complete rotation of the fan, 390 time steps are necessary. Within each time step, an amount of 10 inner iterations is performed. This amount of inner iterations was found to be sufficient to reach convergence of the mass flow and pressure rise over the fan. All unsteady simulations were started from a converged steady-state solution. Convergence was assumed to be reached, when the residuals had dropped below 10^{-4} and the the values for the mass flow through the fan and the pressure rise over it had stabilised. The simulations were performed for three full rotations until the transition from steady-state to unsteady flow behaviour is considered to be done. Then the fan is run for an additional seven rotations, during which the flow field data (velocities, static pressure, temperature) were averaged.

The air was modelled as an incompressible, ideal gas.

Chapter 4

Results and Discussion

In this chapter, the results from the performed studies are presented. In Section 4.1 the three simulation methods are compared to the measurement data from the wind tunnel experiments. In Section 4.2, the simulation results from the pipe-flow study are presented.

4.1 Flow Field Downstream of an Axial Fan

A study of the resulting flow fields from three different fan simulation models is presented in Paper I. The main focus of the paper was on the accuracy in predicting axial velocity component with the three numerical method: MRF, RBM and avgMRF. The simulation results were compared to experimental data obtained by LDA measurements in the model-scale wind tunnel at VCC. The results are once evaluated over a complete wake plane and then along two vertical lines, one in the centreline of the fan and one with a 0.1 m offset, halfway between the root and tip of the blades. The wake plane and the vertical lines are shown in Figure 4.1 as seen from behind.

4.1.1 Axial Velocity Distribution over a Wake Plane

In a first step, the velocities were measured across the whole span of the wake, 0.04 m downstream of the fan shroud. For better visual comparison the CFD results are sampled with the same increments between points as the experimental data (20 x 20 mm).
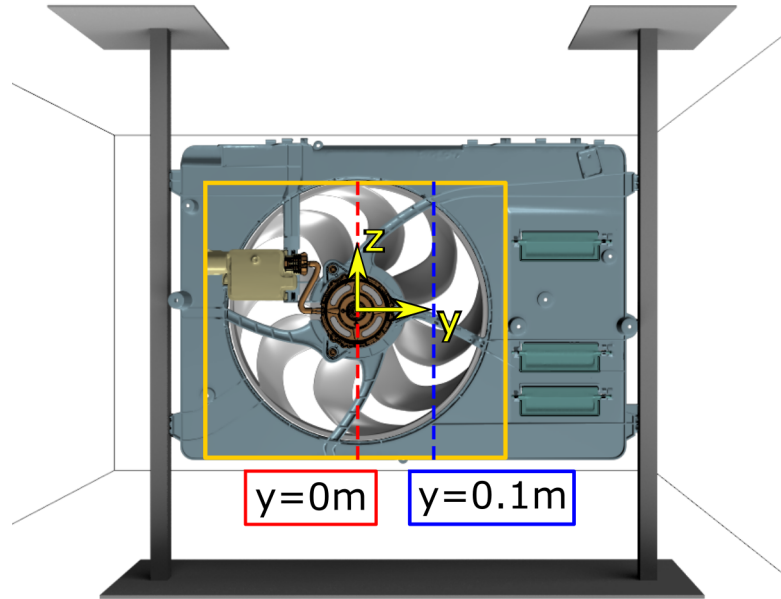
Figure 4.1: *Evaluated sections 0.04 m downstream of the fan, downstream view.*

Figure 4.2 shows the axial velocity field over the wake plane 0.04 m down-stream of the shroud for 1400 rpm (a) and 2800 rpm (b) for the MRF, aver-age MRF and RBM approach and the experimentally obtained axial velocity field. The view is from the downstream direction. The hub, the struts and the control unit in the upper left corner can clearly be identified by the low velocity regions. When comparing the flow fields obtained by the different methods, it is observed that when using the MRF method, the flow field be-comes uneven and the wake of the blades is notable. When using the average flow field over multiple blade positions (avgMRF), this imprint disappears and the flow field becomes more uniform, similar to the resulting flow field from the RBM method and the measurements. However, some differences are still observed. First, there are regions of elevated axial velocity tangentially upstream from the struts (rotation of the air in the MRF zone in clockwise direction). Another difference to the RBM and experimental data is that the velocity close to the control unit is considerably lower in the MRF based approaches. The observations are the same when increasing the rotational rate to 2800 rpm.

(a) *1400 rpm*

(b) *2800 rpm*
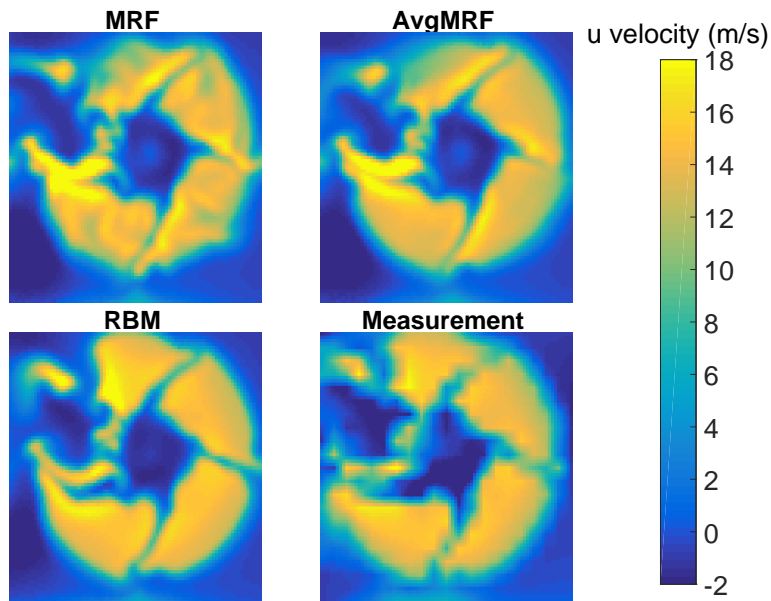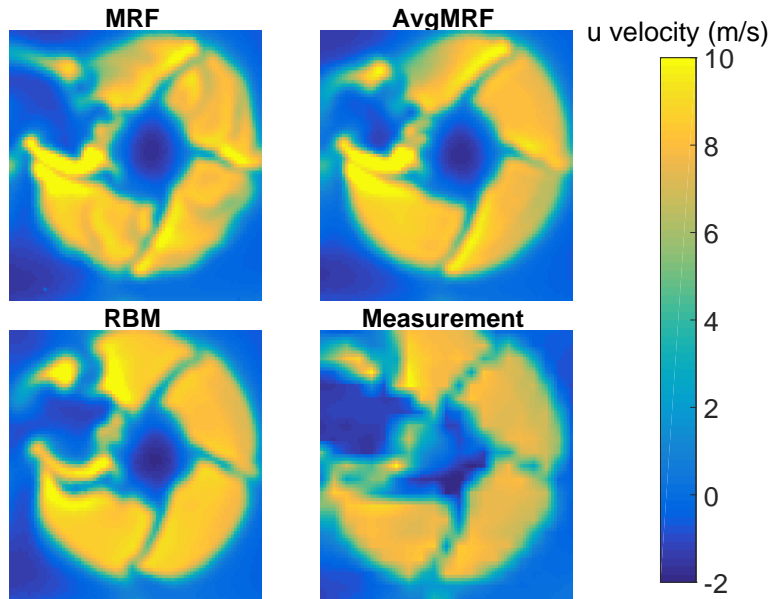
Figure 4.2: *Wake plane 0.04 m downstream of the hub, for the three simulation methods and the experimental results. The view is from behind, the fan rotation is anticlockwise.*
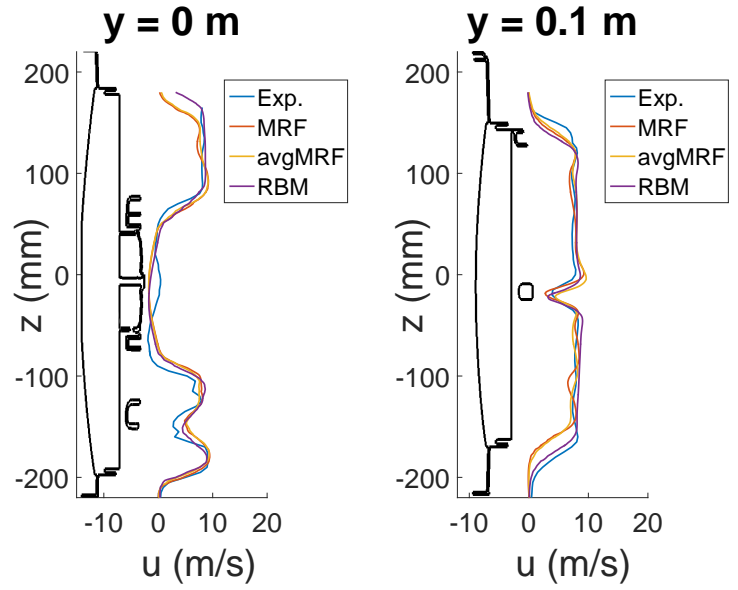
4.1.2 Axial Velocity Profile along Vertical Lines

For a better quantitative comparison, the profile of the axial velocity is measured with smaller increments (5 mm) along two vertical lines (see Fig. 4.1). The data from the CFD simulations is sampled accordingly. The results are shown in Figure 4.3 together with a respective cross sectional view of the fan shroud and fan region. At the low rotational rate (1400 rpm, Fig. 4.3a), the curves for all simulation methods and the experimental results agree well for both lines. Small differences between the measurements and the simulations can be observed downstream of larger structures, such as the hub and the struts, where the seeding might have been insufficient. The velocity profile from the RBM simulation and the experiments show very close agreement, while the MRF based approaches show a significantly lower axial velocity in the area close to the tips. This difference becomes more prominent with an increase in rotational rate (2800 rpm, Fig. 4.3b). Moreover, large fluctuations of the axial velocity can be observed for the standard MRF approach for $y = 0.1$ m for both rates of rotation. This fluctuation can be attributed to the wake of the single blades of the frozen rotor, since their influence disappears when averaging over multiple rotor positions. In Figure 4.3b it can also be observed that both the standard and the averaged MRF approach leads to a peak in axial velocity above the depicted strut ($z \approx 20$ mm), which does not occur for the RBM approach or in the experiments.

4.1.3 Increments for the Average MRF Method

A prerequisite for the average MRF method is that the rotor geometry is rotational symmetric over the interval that is chosen. In the present study, the fan consisted of eight symmetric blades, i.e. the geometry repeated itself every 45°. The results for the averaged MRF method presented in Section 4.1.1 and 4.1.2 were obtained from averaging over 9 positions with a 5° increment. Additionally, a study was performed to investigate if the results can be improved by using a finer increment (45 x 1°) or if a coarser approach could be sufficient (3 x 15°). The results are presented in Figure 4.4. It can be seen that there is no notable difference between using a 1° and a 5° increment. Both the results for the wake plane and the vertical lines look identical for those two cases. With the coarser increment of 15° a slight influence from the blades wake can be seen when looking at the wake plane. Along the centreline the results are almost indistinguishable for all
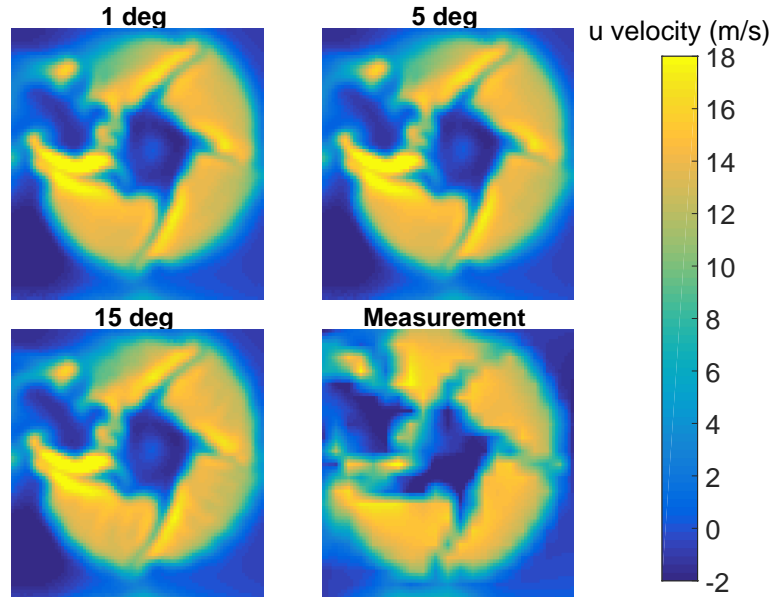
(a) *1400 rpm*
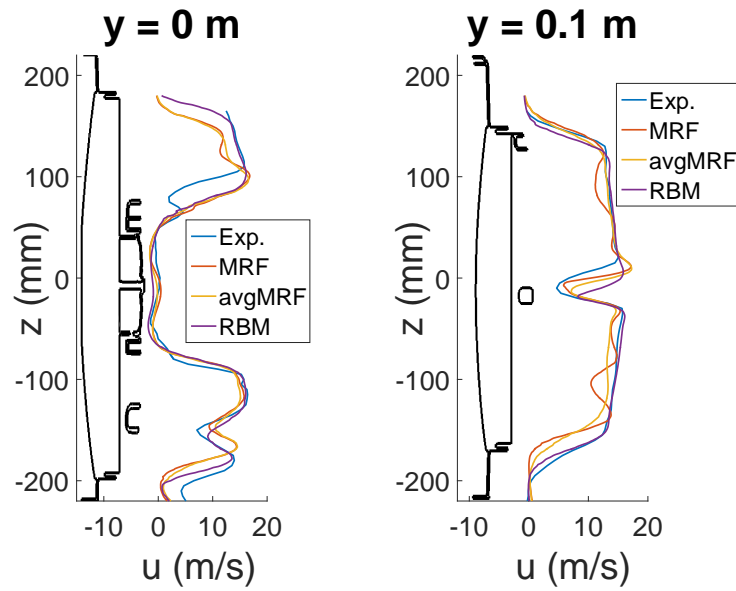
(b) *2800 rpm*

Figure 4.3: *Axial velocity profile 0.04 m downstream of the hub along two vertical lines, for the three simulation methods and the experimental results.*

Figure 4.4: *Wake plane at 0.04 m downstream of the hub, for the avgMRF method performed with three different angle increments compared to the experimental results.*

increments, and only small differences can be observed along the line for $y = 0.1\,\mathrm{m}$. Therefore, the line plots are not presented here.

Hence, depending on the area of application, significant improvements can be achieved by using a few different blade positions instead of just one frozen rotor position.

Conclusions from Paper I

This paper investigated the differences in predicting the flow field between the MRF, RBM and avgMRF method. The results were compared to the axial velocity field measured in the VCC model wind tunnel using LDA. The results obtained from the RBM simulations agreed best with the experimental data. A major issue with the standard MRF methods is that the frozen rotor leaves an imprint in the downstream flow field. This issue was resolved by averaging the flow field over multiple fan positions with the avgMRF approach. However, even when using an averaged MRF approach, there are locations with either unreasonable low velocities (above the control unit) or

unreasonable high velocities (tangentially upstream of the struts and also the control unit). Those effects appear to be inherit to how the MRF approach is transporting properties over the domain and not an effect of the frozen rotor position.

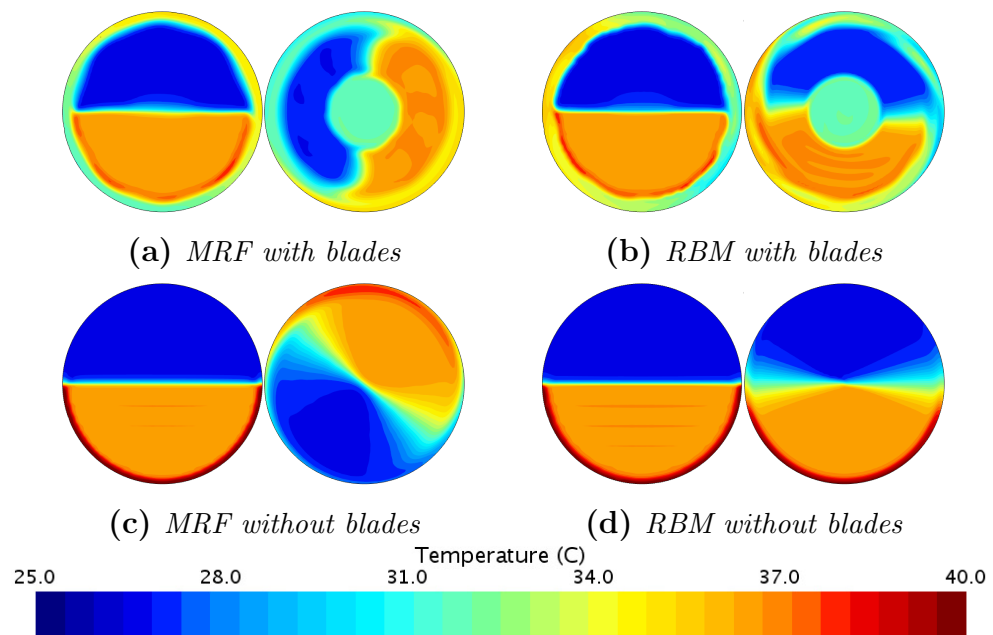## 4.2 Transport of Properties over the MRF Region

The conclusions from Paper I suggest that switching the reference frame to a moving reference frame (MRF) has a non-physical effect on the flow field. Hence, the objective of Paper II is to investigate how different flow properties (temperature, pressure and velocity field) are transported through the MRF zone. For this investigation, the pipe domain described in Section 3.2.2 is used. The investigation is split into two parts: one dealing with how the temperature field is transported, and the second how different obstructions affect the development of the flow field up- and downstream of the MRF zone. This study was purely numerical and used the results from the corresponding RBM simulations as a reference for validation.

4.2.1 Temperature Field

For this investigation, it is studied how the temperature field changes between the upstream interface of the fan zone and the downstream interface. The results for the baseline case ($L_{\mathrm{MRF}} = 60\,\mathrm{mm}$, 2800 rpm) are shown in Figure 4.5, with and without fan blades. The results for a simulation of the same case performed with the RBM approach serve as comparison.

It is observed that when using the RBM approach, the temperature field does not experience any rotation between the upstream and downstream interface. There is a small effect of diffusion that can be observed, but apart from that the temperature field does not move. Looking at the results from the simulations using the MRF approach, it can be seen that in the case with blades, the temperature field experiences a rotation of approximately $90°$, while in the case without the fan blades the degree of rotation is even larger ($\approx 140°$).

An explanation for this rotational effect can be found when looking into the streamlines through the MRF domain (see Fig. 4.6). Since the rotor position is frozen throughout the whole simulation, the streamlines of the absolute

(a) *MRF with blades*

(b) *RBM with blades*

(c) *MRF without blades*

(d) *RBM without blades*

Temperature (C)

25.0   28.0   31.0   34.0   37.0   40.0

Figure 4.5: *Temperature field at the MRF upstream and downstream interfaces for the case with (a) and without blades (c) and the corresponding RBM results (b) and (d).*

(a) *MRF*   (b) *RBM*
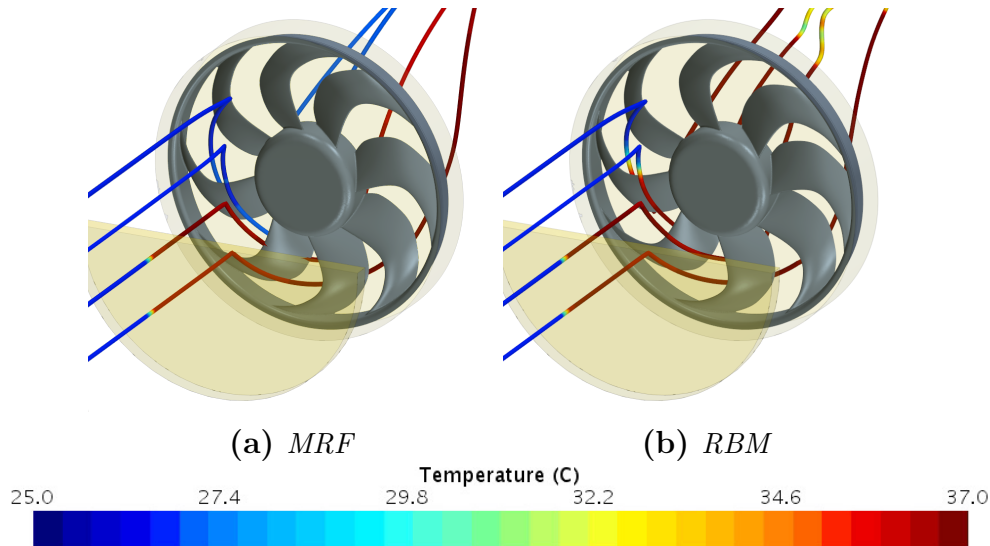
Figure 4.6: *Streamlines of the relative velocity coloured by temperature.*

velocity (i. e. the streamlines in the global reference frame) often collide with the blades. However, the streamlines of the relative velocity use the local reference frame, i. e. they are transformed into the rotating reference frame when entering the MRF region. Figure 4.6 shows the path of four stream-lines of the relative velocity through the fan domain for the MRF (a) and the RBM (b) approach. The streamlines are coloured by temperature. The bottom two streamlines are passing through the heat source, and therefore experience an increase in temperature, while the top two streamlines remain at ambient temperature up to the upstream interface. It can be seen, that when using the MRF approach, the streamlines remain at the same tempera-ture they had when entering the fan domain, while they change temperature according to the local temperature in the global reference frame when using the RBM approach. Hence it can be concluded, that the temperature field is transported by means of the streamlines of the relative velocity in the MRF approach.

Rotational Rate

Since it has been found that there is a significant degree of rotation of the temperature field when using the MRF approach, it is of interest to see how the rotation of the temperature field varies with different rotational speeds of
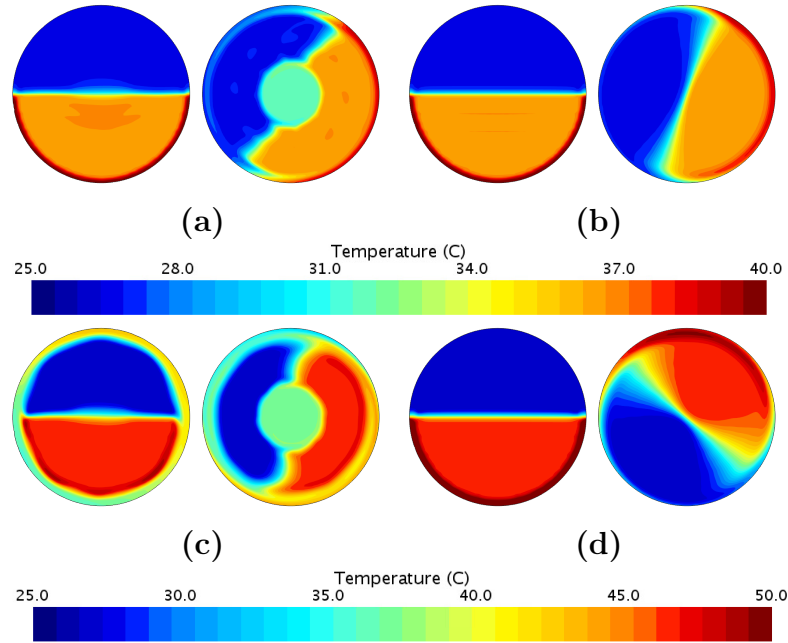
Figure 4.7: *Temperature field up- and downstream of the fan region at a rotational speed of 1400 rpm obtained by an MRF simulation. (a) and (b) at $\dot{m} = 1\,kg/s$ with (a) and without (b) blades, (c) and (d) at $\dot{m} = 0.5\,kg/s$ with (c) and without (d) blades.*

the fan. In case T1, the rotational speed is reduced to 1400 rpm, while keeping the inflow condition and the length of the MRF domain the same as in the baseline case ($L_{\mathrm{MRF}} = 60\,\mathrm{mm}$, $\dot{m} = 1\,\mathrm{kg/s}$, see Table 3.1). The results for the MRF simulation with and without blades can be seen in Figure 4.7a and 4.7b, respectively. The results for the RBM case are not explicitly presented here, since they do not show any change compared to the baseline case, i.e. the temperature field remained un-rotated. Looking at the MRF results, it can be observed that in the case of the bladed region, the temperature field has rotated by $\approx 50\,^\circ$, and in the bladeless region by $\approx 70\,^\circ$. Comparing these degrees of rotation to the baseline case, it can be observed that it has been decreased by approximately half, just as the rotational speed of the fan.

If the mass flow rate is now reduced to half of the baseline case as well ($\dot{m} = 0.5\,\mathrm{kg/s}$), the relation between axial and tangential flow through the fan domain becomes the same as for the baseline case. This case is shown in Figure 4.7c and 4.7d. The degree of rotation is the same as for the baseline

case, hence it can be concluded that the rotation is dependent on the relation between axial velocity (or mass flow rate) and tangential velocity (or rotational rate).

Length of the MRF Domain and Position of the Blades

Next, the influence of the length of the MRF domain on the degree of rotation of the temperature field is investigated. Furthermore, it is examined if there is a notable effect of the distance between up- and downstream interface and the rotor geometry. The results of this study are presented in Figure 4.8. The two columns of figures to the left show the results from an MRF simulation (left: upstream interface, right: downstream interface), while the figures in the column to the far right show the result for the corresponding RBM simulation at the downstream interface.

It is observed that by extending the fan domain from $L_{\mathrm{MRF}} = 60\,\mathrm{mm}$ to $L_{\mathrm{MRF}} = 120\,\mathrm{mm}$, the degree of rotation has doubled from $\approx 90\,°$ to now $\approx 180\,°$. This means, that the areas that should only experience the ambient temperatures are now facing higher temperature levels and vice versa. The placement of the blades in relation to the interfaces only has a comparatively small impact on the rotation of the temperature field. Between (a) and (b) as well as between (b) and (c) the rotation of the temperature field is approximately $10\,°$.

4.2.2 Flow Field

In a next step, it is investigated how changes in the flow field are being transported through the MRF domain. For this study, three obstacles were introduced to the flow. First a cylinder placed in close vicinity to the upstream MRF interface (case F1), then the same cylinder placed close to the downstream interface (case F2), as well as a box placed downstream of the MRF region (case F3). All cases have a MRF domain with length $L_{\mathrm{MRF}} = 60\,\mathrm{mm}$ and the rotational rate is set to $2800\,\mathrm{rpm}$ (see Table 3.1). The position of the upstream and downstream MRF interfaces are $x = -0.32\,\mathrm{m}$ and $x = 0.28\,\mathrm{m}$, respectively.

(a) *Blades placed close to the upstream interface*

(b) *Blades placed in the centre of the domain*

(c) *Blades placed close to the downstream interface*
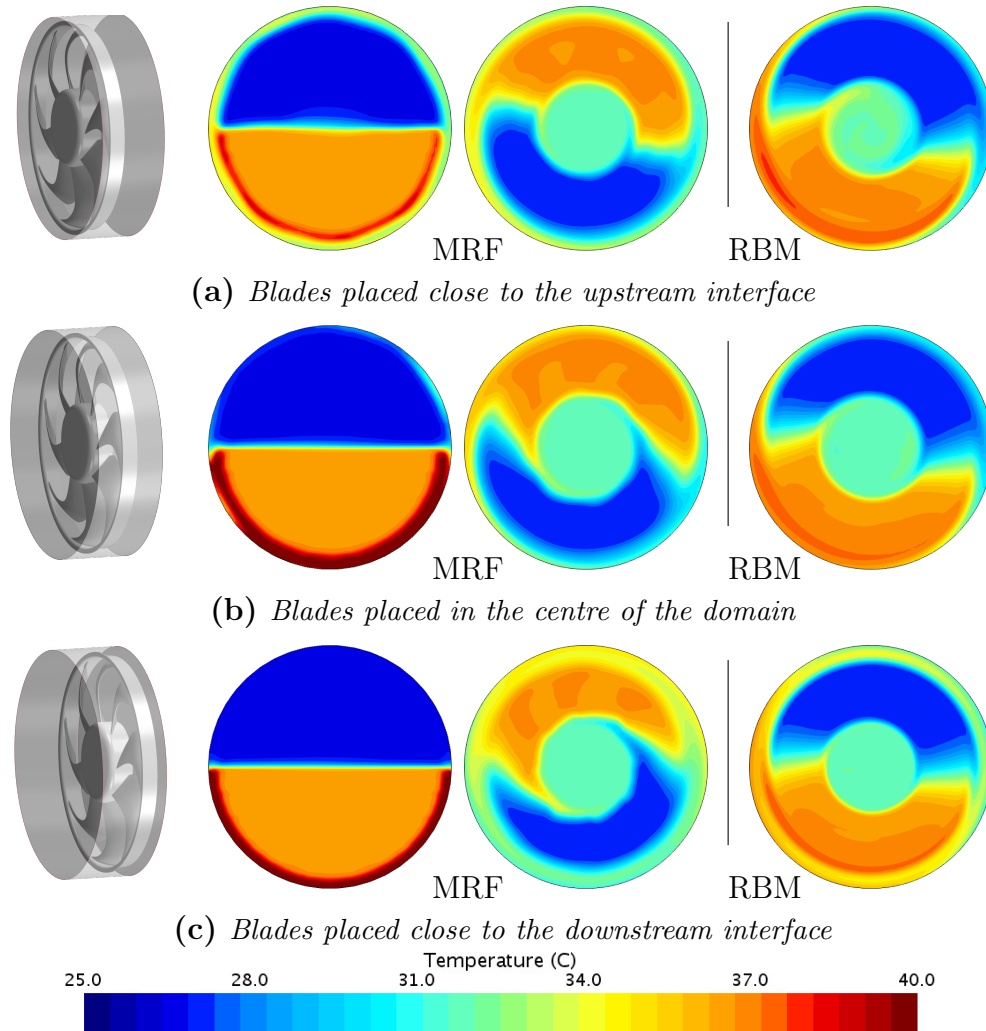
Figure 4.8: *Temperature field up- and downstream of the fan region for varying fan blade positions in respect to the interfaces performed with the MRF (middle) and RBM approach (right). The length of the fan region is $L_{MRF} = 120\,mm$ and the fans rotational speed is 2800 rpm.*
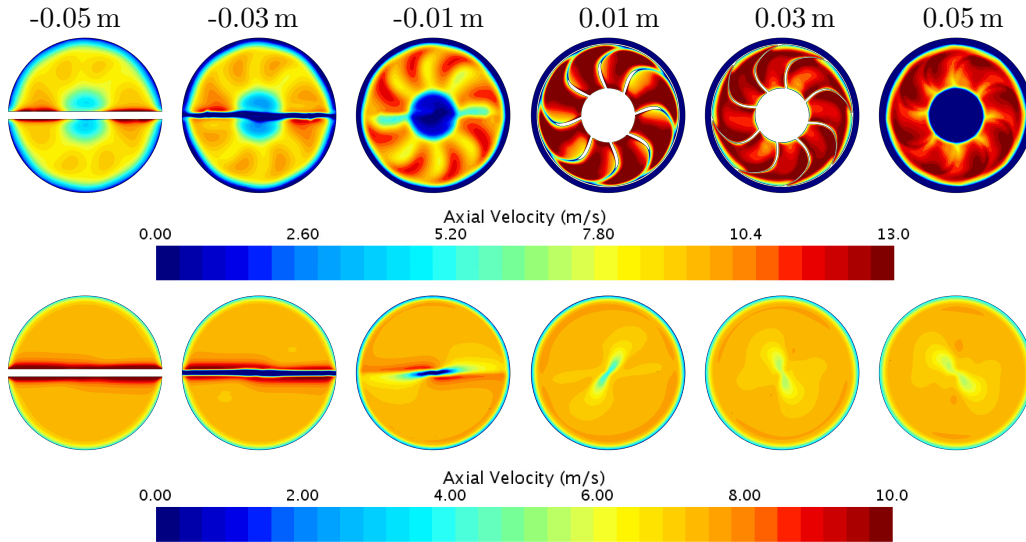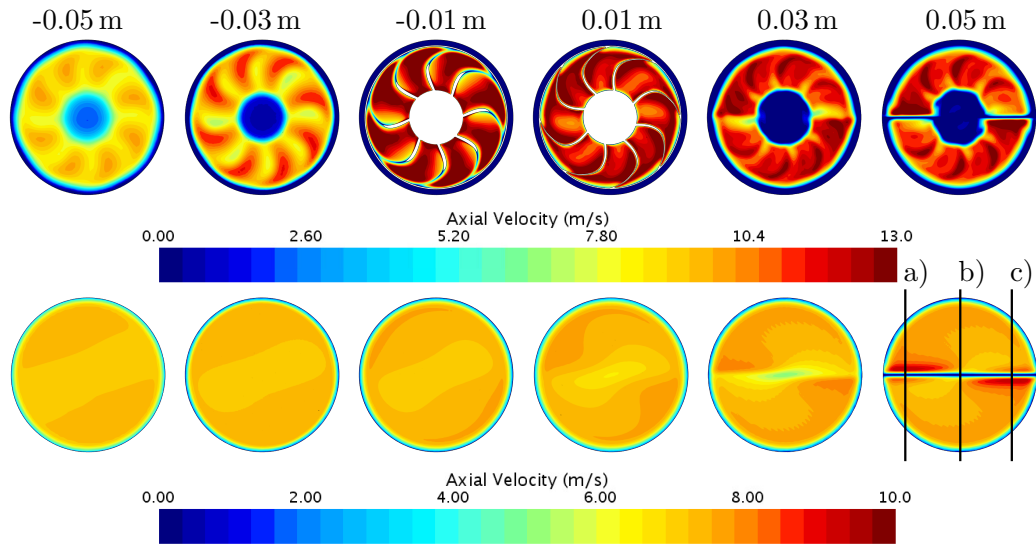
Figure 4.9: *Influence of a cylinder placed upstream of the MRF region with (upper row) and without blades (lower row) on the axial velocity field from 0.05 m upstream (left) to 0.05 m downstream (right) of the blades.*

F1 – Upstream Cylinder

Figure 4.9 shows the axial velocity distribution over the pipes cross section from 0.05 m upstream to 0.05 m downstream of the fan blades (from left to right) for the case with and without blades run with the MRF approach.
In the case without fan blades, it can be observed that the wake of the cylinder is rotated through the MRF domain, even though there is no physical reason for this behaviour. The degree of rotation is the same as for the temperature field ($\approx 140\,°$). When the fan blades are in place, the rotation of the wake can be followed until $x = 0.01\,\text{m}$. Then the effect from the blades destroys the wake of the cylinder, and no trace is left downstream of the MRF domain ($x = 0.05\,\text{m}$).

F2 – Downstream Cylinder

Placing the cylinder downstream of the MRF region depicts a different behaviour than in case F1. As can be seen in Figure 4.10, there is a small effect on the axial velocity in the upstream region that can be observed in the case without blades. This effect, however, is too small to be noted in the case with fan blades further upstream than $x = 0.03\,\text{m}$. It appears that there is a rotation in the flow field of the axial velocity as well, but this rotation

Figure 4.10: *Influence of a cylinder placed downstream of the MRF region with (upper row) and without blades (lower row) on the axial velocity field from 0.05 m upstream (left) to 0.05 m downstream (right) of the blades.*

seems to have taken place between the cylinder and the downstream MRF interface. Once inside the MRF region, the orientation of the flow field does not change. In order to understand the origin of this effect, it is necessary to look at the distribution of the static pressure and its interaction with the flow in the MRF region. This is presented in Figure 4.11 for the case without a rotor geometry in the MRF domain. This figure shows the static pressure field and the projected streamlines of the relative velocity on a plane for an x-z-cross section for $y =$0.15, 0 and $-$0.15 m (marked (a)-(c) in Figure 4.10). It is observed that in areas where the pressure field originating from the cylinder reaches into the MRF domain, the streamlines are notably slowed down. This means for case (a), for example, that the absolute velocity of the streamlines exiting the MRF zone above the cylinder will be significantly higher than the velocity of the streamlines passing through the high pressure zone and decelerating. In the centreplane ($y = 0$ m, (b)), there is no rotation in the MRF domain, and the static pressure field also does not reach as far into the MRF domain than in location (a). Therefore, the distribution is more uniform. In the third case (c), the flow in the MRF domain comes from below, therefore creating a lower velocity above the cylinder. This imbalance can also be observed in Figure 4.10, second row, first picture from the right.

(a) $y = 0.15\,m$


(b) $y = 0\,m$

(c) $y = -0.15\,m$
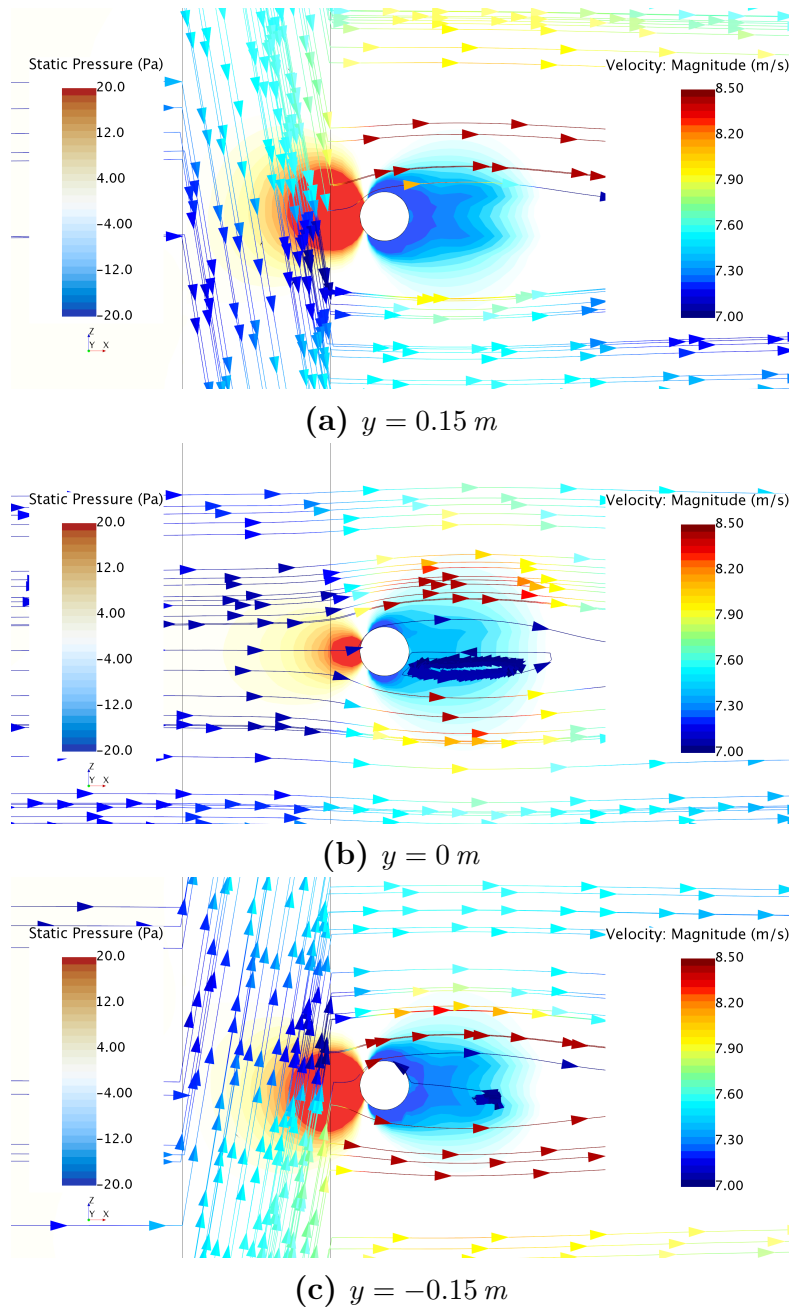
Figure 4.11: *Longitudinal view of the static pressure field and streamlines of the relative velocity coloured by magnitude, for case F2 (downstream cylinder) without fan blades. (a) left hand, (b) centre and (c) right hand plane (compare Figure 4.10).*

F3 – Downstream Box

The last object investigated is a box placed downstream of the MRF region. This object was chosen due to the effects of large objects on the flow field that was seen and described in Paper I and Section 4.1.1. Figure 4.12 shows the axial velocity field from 0.05 m upstream of the blades to 0.05 m downstream of them for the MRF simulation of the case with (upper row) and without (lower row) rotor geometry. It can be seen that, even with the blade geometry in the fan zone, the box has a notable effect on the flow field upstream of the MRF zone. In the case without blades, this effect can be seen as well, but a more notable effect is the imbalance in axial velocity that is created close to the box. The closer one gets to the location of the box, one can notice that the velocities in the lower right half are considerably higher than in the upper left half. This can be explained when looking at the distribution of the static pressure around the box and the projected streamlines of the relative velocity through the MRF domain (Figure 4.13). Just as in case F2 (downstream cylinder) the pressure field propagates into the MRF domain and causes the streamlines there to decelerate. Given that the sense of rotation of the air in the fan zone is anticlockwise (since the sense of rotation of the fan is clockwise), the streamlines exiting the MRF zone before passing the high pressure zone will have a considerably higher velocity than the streamlines that are decelerated due to the elevated pressure caused by the presence of the box.
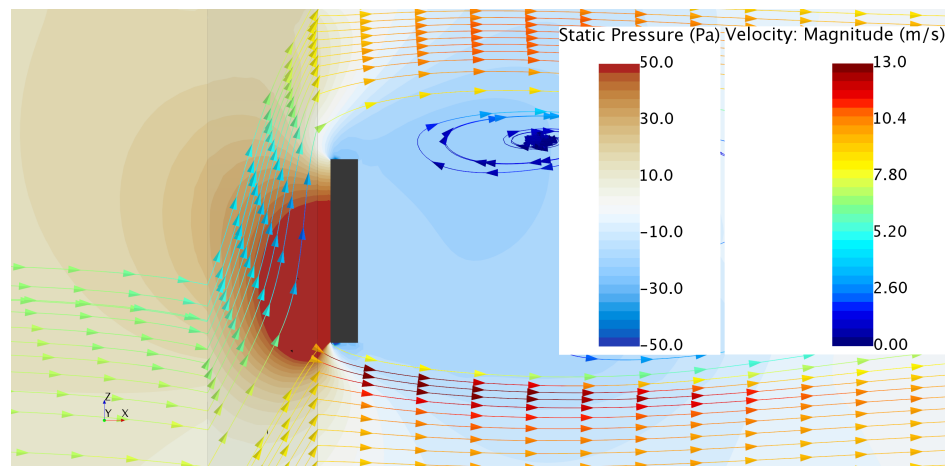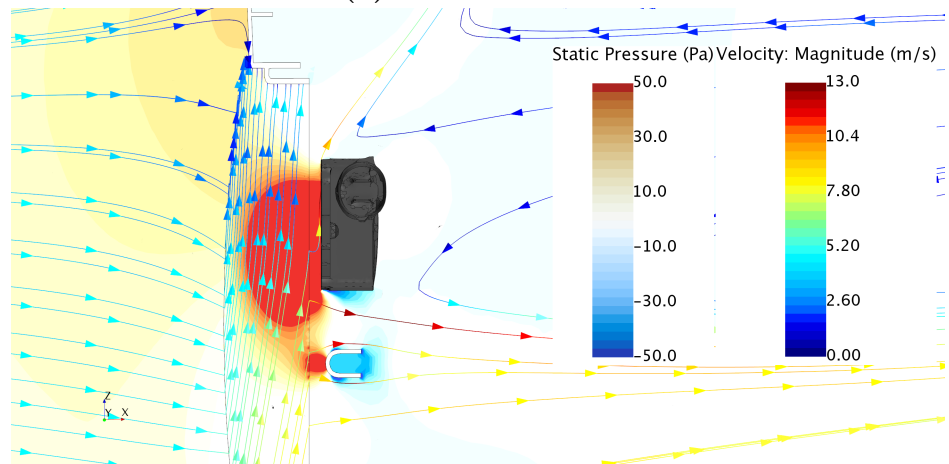
4.2.3   Conclusions from Paper II

In this study it has been found, that the temperature field and velocity vectors are rotated when passing through an MRF domain. This is due to the fact that the streamlines of the velocity in the (stationary) global reference frame often collide with the frozen rotor position, and information would get lost in the process. Therefore, the properties in the MRF region are transported with the streamlines of the relative velocity instead. As could be shown, this leads to a non-physical rotation of all disturbances from the upstream direction, even for set-ups without any blade geometry in the MRF zone. The degree of rotation was shown to be dependent on the length of the MRF domain, the operating point and the blade geometry itself. In the respective RBM simulations, no rotation was observed. Downstream obstacles have an influence on the upstream flow field by causing an increase
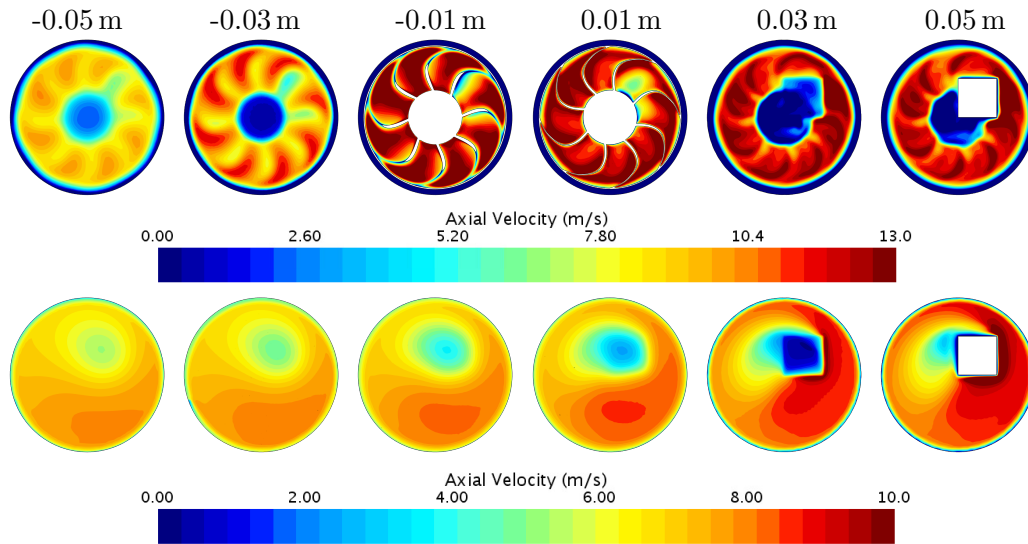
Figure 4.12: *Influence of a box placed downstream of the MRF region with (upper row) and without blades (lower row) on the axial velocity field from 0.05 m upstream (left) to 0.05 m downstream (right) of the blades.*

in static pressure. If this increased pressure field reaches into the fan zone, the relative streamlines are decelerated in the fan region, causing an imbalance in the flow field up- and downstream of the fan region.

(a) *Downstream Box*

(b) *Control unit from Paper I*

Figure 4.13: *Static pressure field and constrained streamlines of relative velocity coloured by velocity magnitude.*

Chapter 5

Conclusions

The purpose of this thesis has been to present and investigate the possibilities and limitations of different ways of modelling the rotation of an axial cooling fan in CFD. The presented methods were the *Multiple Reference Frame (MRF)* model, the *Rigid Body Motion (RBM)* model and a hybrid MRF approach, which was in this study referred to as the *Average MRF (avgMRF)* method.

In a first study, the three numerical approaches were compared to each other and to experimental data for an isolated production fan in its shroud. The comparison was done for the axial velocity profile in one cross sectional plane downstream of the fan, as well as along two vertical lines in the same plane. This study was performed for two different fan speeds at constant wind tunnel inlet velocity. The experimental data was obtained by performing Laser Doppler Anemometry (LDA) measurements. The results showed, that the RBM model had the best ability of reproducing the measurement data, while the standard MRF approach showed large deficits, amongst others due to the frozen rotor position. The frozen rotor position was seen to affect the flow, by leaving an imprint caused by the wake of the stationary blades. The averaged MRF method was able to remove the imprint from the rotor and provided a more uniform flow field, which was closer to the RBM and experimental results. However, the areas around large structures (the struts and the control unit) still showed large differences in axial velocity magnitude, which could not be explained by the frozen rotor position. Nevertheless, it was shown that using multiple rotor positions for the MRF approach can provide improved flow field results at a low computational cost.

The second study aimed at improving the understanding of how flow properties are treated and transported in an MRF region. The investigation was purely numerical and the RBM approach, which had previously shown to provide physically accurate results, was chosen as a reference case. The computational domain was a circular pipe, slightly larger than the fan diameter, and the MRF zone stretched over the complete cross section. First, a heat source was introduced upstream to the fan region. It was found that the thereby created high temperature field is rotated when passing through the MRF domain, while it is not rotated in the RBM simulation. The rotation through the MRF region even occurred when there was no blade geometry present in the fan region, and therefore clearly represents a non-physical behaviour. It was found that the degree of rotation is dependent on the length of the MRF zone, the ratio between axial and tangential velocity component and the presence of the blades. Second, the interaction between different geometrical obstacles and the flow through the MRF zone was studied. It was found that disturbances in the upstream flow field are rotated by the same degree of rotation as the temperature field. When the blade geometry was present in the MRF zone, smaller disturbances were superposed by the wake of the blades, so that no notable influence could be seen in the downstream flow field. Geometries placed downstream of the MRF zone, showed a different kind of influence on the upstream flow field. Given that the geometries are placed in close proximity to the MRF interface, the increase in static pressure reaches into the MRF domain, thereby decelerating the rotating flow in the MRF zone. The effect can be seen by an imbalance in velocity magnitude, dependent on the size of the obstacle. Furthermore, this also presents the explanation for differences between the axial flow field around the struts and the control unit that was observed in the first study. Concluding, it has been confirmed that the Rigid Body Motion approach gives the most physical results for flows with rotating geometries, and agrees best with experimental data. The MRF approach has some severe limitations and should be used with care, especially when there are large temperature differences in the upstream flow field. The switching in reference frame, from a stationary to a rotating one and back, causes non-physical behaviour in the transport of field properties which is not being compensated for. Whenever the computational resources allow it, the RBM approach should be preferable to the MRF. In situations that do not allow for using the RBM approach, the average MRF method can help to improve the flow field prediction, by removing the blade imprint from the wake.

5.1   Future Work

With the present work, first steps have been taken into further improving the understanding of underhood flow, by investigating the possibilities and limitations of the simulation of the axial cooling fan. This is important and useful, since the cooling fan is the driving force in the engine bay, and the accuracy of the predicted flow distribution in the complete underhood environment is largely dependent on the correct initial conditions.

However, the studies so far have been limited to the axial velocity component only. With a recently purchased 3-D LDA set-up, the comparisons between the fan models will be extended to the radial and tangential velocity component as well, to get a the complete flow field information downstream of the fan.

In a next step, the complexity of the set-up will be increased in order to create a set-up that is closer to an actual underhood compartment. So far, the fan has been operating in a stand-alone configuration, with only minor geometries, such as struts or a control unit, around it. In the narrow underhood environment large components, such as heat exchangers, the engine or other auxiliary devices can be found in close proximity. Those components will have a large impact on the fans operating conditions, and hence on the flow entering the underhood domain. Furthermore, the accuracy of the flow field prediction downstream of the fan might also have an impact on whether the flow is taking the same path as in reality. This shall be investigated numerically and experimentally.

Finally, the aim is to perform measurements in relevant areas in the underhood of a complete vehicle and be able to compare those to simulation data.

Bibliography

[1] AMEA, *New Passenger Car Registrations By Alternative Fuel Type in the European Union*, Tech. Report April, 2019.

[2] T. Anthoine, T. Arts, H. Boerrigter, J.-M. Buchlin, M. Carbonaro, G. Degrez, R. Dénos, D. Fletcher, D. Olivari, M. Riethmuller, and R. Van den Braembussche, *Measurement Techniques in Fluid Dynamics - An Introduction*, 2009.

[3] H. Berneburg and A. Cogotti, *Development and Use of LDV and Other Airflow Measurement Techniques as a Basis for the Improvement of Numerical Simulation of Engine Compartment Air Flows*, SAE Technical Paper, (1993).

[4] A. Cogotti, *Engine Compartment Airflow Investigations Using a Laser-Doppler-Velocimeter*, SAE Technical Paper, (1991).

[5] M. B. Dogruoz and G. Shankaran, *Computations with the multiple reference frame technique: Flow and temperature fields downstream of an axial fan*, Numerical Heat Transfer; Part A: Applications, 71 (2017), pp. 488–510.

[6] D. Dynamics, *BSA Flow Software User Guide Documentation, Version 6.50.00.41*, 2017.

[7] J. Foss, D. Neal, M. Henner, and S. Moreau, *Evaluating CFD Models of Axial Fans by Comparisons with Phase-Averaged Experimental Data*, SAE Technical Paper Series, 1 (2001).

[8] P. Gullberg and L. Löfdahl, *Fan Modelling in CFD Using MRF Model For Under Hood Purposes*, in Proceedings of the ASME-JSME-KSME Joint Fluids Engineering Conference 2011, Hamamatsu, 2011.

[9] P. Gullberg, L. Löfdahl, S. Adelman, and P. Nilsson, *A Correction Method for Stationary Fan CFD MRF Models*, SAE Technical Paper Series, 1 (2009).

[10] ——, *An Investigation and Correction Method of Stationary Fan CFD MRF Simulations*, SAE Technical Paper Series, 1 (2009).

[11] P. Gullberg, L. Löfdahl, and P. Nilsson, *Cooling Airflow System Modeling in CFD Using Assumption of Stationary Flow*, SAE Technical Paper Series, 1 (2011).

[12] P. Gullberg and A. Tavernier, *Modeling of Closed Fans using CFD and Steady State Assumption of Fluid Flow*, SAE Technical Paper Series, 1 (2014).

[13] P. V. Gullberg, *Optimisation of the Flow Process in Engine Bays - 3D Modelling of Cooling Airflow*, phd thesis, Chalmers University of Technology, 2011.

[14] T. Hobeika, P. Gullberg, S. Sebben, and L. Lofdahl, *Force Based Measurement Method for Cooling Flow Quantification*, SAE International Journal of Passenger Cars - Mechanical Systems, 10 (2017), pp. 619–627.

[15] T. Hobeika and S. Sebben, *CFD investigation on wheel rotation modelling*, Journal of Wind Engineering and Industrial Aerodynamics, (2018).

[16] M. Khaled, M. Gad El Rab, F. Hachem, H. Elhage, A. El-marakbi, F. Harambat, and F. Peerhossani, *Experimental Study of the Flow Induced by a Vehicle Fan and the Effect of Engine Blockage in a Simplified Model*, International Journal of Automotive Technology, 13 (2016), pp. 293–300.

[17] M. Khaled, F. Mangi, H. E. Hage, F. Harambat, and H. Peerhossaini, *Fan air flow analysis and heat transfer enhancement of vehicle underhood cooling system - Towards a new control approach for fuel consumption reduction*, Applied Energy, 91 (2012), pp. 439–450.

[18] Y. Kobayashi and I. Kohri, *Study of Influence of MRF Method on the Prediction of the Engine Cooling Fan Performance*, SAE Technical Paper, (2011).

[19] I. Kohri and Y. Kobayashi, *Prediction of the Performance of the Engine Cooling Fan with CFD Simulation*, SAE Int. J. Passeng. Cars - Mech. Syst., 3 (2010), pp. 508–522.

[20] T. Kuthada, *A Review of Some Cooling Air Flow Measurement Techniques for Model Scale, Full Scale and CFD*, SAE International Journal of Passenger Cars - Mechanical Systems, 6 (2013), pp. 88–96.

[21] S. T. J. Lien and N. A. Ahmed, *Numerical simulation of rooftop ventilator flow*, Building and Environment, 45 (2010), pp. 1808–1815.

[22] S. M. Lim, A. Dahlkild, and M. Mihaescu, *Aerothermodynamics and exergy analysis of a turbocharger radial turbine integrated with exhaust manifold*, in Proceedings of the 13th International Conference on Turbochargers and Turbocharging, London, 2018, KTH, Fluid Physics.

[23] S. H. Liu, R. F. Huang, and C. A. Lin, *Computational and experimental investigations of performance curve of an axial flow fan using downstream flow resistance method*, Experimental Thermal and Fluid Science, 34 (2010), pp. 827–837.

[24] E. Ljungskog, *Investigations of Flow Conditions in an Automotive Wind Tunnel*, licentiate, Chalmers University of Technology, 2017.

[25] Z. Lyu and P. Aurora, *Aerodynamic Wind Tunnel in Passenger Car Application*, tech. report, 2016.

[26] E. Y. Ng, S. Watkins, P. W. Johnson, and L. Mole, *Measuring Local Time-Averaged Airflow Velocity through an Automotive Heat Exchanger*, (2001), pp. 517–520.

[27] W. Peng, G. Li, J. Geng, and W. Yan, *A strategy for the partition of MRF zones in axial fan simulation*, International Journal of Ventilation, 3315 (2018), pp. 1–15.

[28] G. V. Shankaran and M. B. Dogruoz, *Validation of an advanced fan model with multiple reference frame approach*, 2010 12th IEEE Intersociety Conference on Thermal and Thermomechanical Phenomena in Electronic Systems, ITherm 2010, (2010), pp. 1–9.

[29] Siemens, *Simcenter StarCCM+ Documentation*, 2019.

[30] H. Versteeg and W. Malalasekera, *An Introduction to Computational Fluid Dynamics : The Finite Volume Method*, Harlow: Pearson Prentice Hall, 2 ed., 2007.

[31] A. Wang, Z. Xiao, and H. Ghazialam, *Evaluation of the Multiple Reference Frame (MRF) Model in a Truck Fan Simulation*, SAE Technical Paper Series, 1 (2005).

[32] A. Wäschle, *Numerische und experiementelle Untersuchung des Einflusses von drehenden Rädern auf die Fahrzeugaerodynamik*, Expert Verlag, 2006.

[33] ——, *Numerische und experimentelle Untersuchung des Einflusses von drehenden Rädern auf die Fahrzeugaerodynamik*, phd thesis, University Stuttgart, 2006.

[34] F. Zenger, C. Junger, M. Kaltenbacher, and S. Becker, *A Benchmark Case for Aerodynamics and Aeroacoustics of a Low Pressure Axial Fan*, SAE Technical Paper Series, 1 (2016).

[35] Z. J. Zhai, Z. Zhang, W. Zhang, Q. Y. Chen, Z. J. Zhai, and Q. Y. Chen, *Evaluation of Various Turbulence Models in Predicting Airflow and Turbulence in Enclosed Environments by CFD : Part 1 Summary of Prevalent Turbulence Models Evaluation of Various Turbulence Models in Predicting Airflow and Turbulence in Enclosed Environ*, HVAC&R Research, 13 (2007), pp. 853–870.

[36] L. Zhao, W. Chen, S. Liu, H. Zhang, J. Liu, Y. Gao, and E. Arens, *Experimental and numerical investigations of indoor air movement distribution with an office ceiling fan*, Building and Environment, 130 (2017), pp. 14–26.